On the Variability of Equatorial Electrojet During Geomagnetic Quiet Conditions

BY

MASAD QAYYUM

A dissertation submitted in partial fulfillment of the

requirements for the degree of

MASTER OF PHILOSOPHY

IN

PHYSICS

Department of Physics

Quaid-i-Azam University, Islamabad, Pakistan

December 13, 2023

Declaration

This is to certify that the research work presented in the thesis, entitled " On the Variability of Equatorial Electrojet During Geomagnetic Quite Conditions " was conducted by Mr. Masad under the supervision of Dr. Majid Khan and accepted in present form by Department of Physics, Quaid-i-Azam University, Islamabad as satisfying dissertation requirement for the degree of

MASTER OF PHILOSOPHY IN PHYSICS

Supervisor

Dr. Majid Khan
Associate Professor

Submitted through

Prof. Dr. Kashif Sabeeh
Chairperson
Department of Physics
Quaid-i-Azam University
Islamabad, Pakistan

Abstract

The ionosphere constitutes an ionized uppermost layer of the atmosphere, possessing significant importance in facilitating satellite and radio communications. In particular, the navigation and communication systems may suffer if the density of ionized particles in this region is disturbed. Although many factors can affect the ionosphere, our current investigation is focused on the Equatorial Electrojet (EEJ). This phenomenon is caused by a concentrated flow of intense electric current down the dip-equator's day-side in the so-called E region of the ionosphere. The configuration of the Earth's magnetic field, which includes horizontally oriented field lines throughout certain latitudes, is the primary factor for the increase in such current density. This occurrence results in a considerably elevated level of electrical conductivity within a specific segment of the ionospheric E layer, spanning roughly 600 km across a latitudinal extent. Because of this, even weak electric fields in the vicinity can cause considerable currents to flow inside this particular location. Here in this study, we first present the historical findings that were crucial in identifying the EEJ, following that we provide a brief overview of the distinctive features displayed by the said index. This involves its seasonal fluctuations, daily variations, and its connection with the Solar Sunspot Number (SSN).

For our analysis, we employ the off-equatorial subtraction method for effectively isolating the unique magnetic signal – associated with EEJ – from other variations at the respective geomagnetic observatories. By utilizing data from both equatorial and off-equatorial observatories, the EEJ is accurately evaluated. For that, we only use information from quiet days and eliminate the other data by writing our MATLAB program/scripts. The data sets were used from the INTERMAGNET database, where observatories are encouraged to produce data with resolutions as low as one minute or even one second, recording variations in the magnetic field over brief time intervals.

For our investigations, we implemented a dataset that included the years 2018 through 2022. We started by extracting EEJ signals from this dataset. Then, we carried out an extensive analysis to identify multiple features related to the EEJ signals. These

features include the asymmetry between winter and summer behavior, as well as the diurnal and seasonal variations of the EEJ. In the study of daily fluctuations, we observe a pattern where the intensity of the EEJ starts from zero in the early morning, gradually gains strength, and reaches its highest value between 11 to 13 LT. Following this, it gradually weakens, with its lowest point occurring during late night hours. Also, we find out that EEJ density is maximum during the December and June solstice seasons, showing annual asymmetry. To uncover potential connections and inter-dependencies, we also delved into the correlation between the EEJ and SSN. Our findings indicate that EEJ shows a direct dependency on the SSN index, i.e. the former increases with the later. This thorough analysis can provide a better understanding by shedding light on the complex dynamics of the EEJ phenomena during this particular period.

Acknowledgment

First of all, I want to start by thanking Allah Almighty for guiding me through hardships and for being a constant in my life. I extend my sincerest appreciation to my mentor and supervisor, Dr. Majid Khan, whose remarkable ability to inspire and uplift has broadened my intellectual horizons as a student. His unswerving support, dedication to our work, and scholarly guidance have played a pivotal role in the completion of this dissertation. I would also like to convey my deepest thanks to Mr. Waqar Younas, whose precious time and invaluable insights have been instrumental in shaping the direction of my research. His expert advice and constructive feedback have been crucial elements in the successful execution of my study. The expression of gratitude would be insufficient if I fail to recognize the invaluable contributions of my beloved parents (Abdul Qayyum Khan & Tahira Taskeen). Their prayers have consistently illuminated my path, and their unending support has opened numerous doors for me. My father always motivates me and serves as a backbone of support for me. Their sacrifices and efforts have exceeded all expectations, and I am profoundly grateful for their unwavering faith in me. I would like to express my gratitude to my colleague, Iqra Raza, whose invaluable assistance has been a constant throughout this year. I also want to extend my heartfelt appreciation to my siblings and friends for their unwavering presence and unwavering support at every stage of this journey.

Contents

List of Figures

List of Tables

Chapter 1

Introduction

1.1 Ionosphere

The ionized part of the Earth's upper atmosphere which extends from roughly 60 kilometers (37 miles) to 1,000 kilometers (621 miles) in the magnetosphere. The interaction of solar radiation and cosmic radiations with the upper atmosphere of the Earth creates the ionosphere. The sun radiates a variety of electromagnetic radiations, e.g. ultraviolet (UV), X, and gamma rays, which can ionize neutral atoms and molecules in the Earth's upper atmosphere [6]. The electric and magnetic fields can influence the motion of these ionized particles resulting in a plasma-like environment in the upper atmosphere. A number of variables – including solar activity, geomagnetic activity, and atmospheric conditions – have an impact on the ionospheric formation. For example ionosphere can become highly ionized during periods of a strong solar activity, such as solar flares or coronal mass ejections [7], during times of geomagnetic activity, such as magnetic storms, satellite-based communication and navigation systems might suffer [8]. Depending on the ionization properties and latitude, the ionosphere is divided into several layers. The absorption of solar energy by ionized molecules and atoms is the main process by which the lower layers, such as the D and E layers, are created. With the help of additional ions and the free electrons released during the absorption process, plasma is created. Atomic Oxygen is ionized by solar radiation to produce the higher layers of the ionosphere, such as the F1 and F2 layers [9].

1.2 Ionospheric variations

The ionosphere is a dynamic medium, and as such, its properties change throughout time. This implies that a good communication link cannot be established using a single radio frequency continuously throughout the year, or even, throughout the day. Variations in the ionosphere's characteristics are affected by the solar cycle, seasons, location, and time of day. Consequently, a frequency that may be effective for communication at one moment may not be at another counterpart [10].

The ionosphere's capacity to permit communication between various sites on the Earth's surface may be significantly impacted by these changes. The following are some of the main variables that have an impact on the ionospheric dynamics.

1.2.1 Solar cycle variations

Solar cycles, a recurring pattern of rising and falling activity on the Sun, have an effect on high-frequency (HF) communications. These cycles normally span nine to fourteen years. The HF signals cannot travel through the ionosphere when there is little solar activity [11], only the lower frequencies can. However, HF modes can effectively travel at times of peak solar activity because the increased radiation from the sun creates more electrons in the ionosphere, allowing for their passage [12].

1.2.2 Seasonal variations

Different ionospheric fluctuations have an impact on it's characteristics and on their capacity for communication between two sites on Earth. For example summer has greater plasma frequencies than winter does in the E region. While in the F region frequency fluctuation is more complicated and has a peak in both hemispheres near the respective equinoxes. The noon frequencies in summer are generally greater than those during winter in the solar minimum. Winter frequencies, however, may be greater than summer counterparts in some places during a maximum solar activity. Furthermore, regardless of solar activity, the frequencies around the equinoxes are higher than those in the summer or the winter [13]. The seasonal anomaly is the name given to this seasonal difference in frequencies, with winter noon frequencies exhibiting larger values.

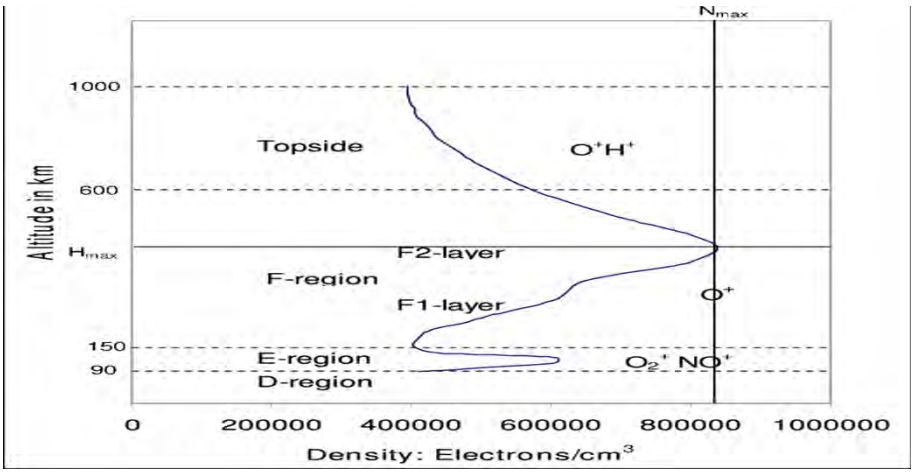

Figure 1.1: The variations of electron number density in different ionospheric layers.

1.2.3 Altitudinal variation

1.2.3.1 Layers of ionosphere

Based on its height and degree of ionization the ionosphere has been divided into many layers, [14] each of which has distinct features and impacts on radio propagation and other atmospheric processes as illustrated by Fig.1.1. In the following we briefly discuss these regions.

1.2.3.2 D layer

At a height of around $60 - 90km$ above the surface of the planet, the D layer is located, which is the lowest ionospheric region [15]. It is created when ionized molecules and atoms, such as nitrogen and oxygen, absorb solar light. As a result, they become excited and lose their electrical charge. The interaction of high-energy solar particles like X-rays and UV light with the atmosphere's neutral atoms and molecules results in the ionization, e.g. one electron can be removed from a nitrogen molecule in the Earth's atmosphere leaving a positively charged nitrogen ion and a free electron. When such a free electron strikes a neutral molecule, it might knock off another electron, producing a new positively charged ion, its called the secondary ionization. A layer of ionized particles is eventually formed in the Earth's atmosphere as a result of this process, which keeps going.

The D layer may also be influenced by other atmospheric and meteorological phenomena, for instance, it may move upward/downward due to temperature inversions in the atmosphere, and it may also be temporarily disturbed by ionospheric disturbances brought on by thunderstorms. Overall, a complex interaction of elements, such as solar

radiation, geomagnetic storms, and other atmospheric and meteorological phenomena, affect the density and behavior of the D layer in the ionosphere.

It may be challenging for radio waves to travel over great distances because plasma particles cause them to weaken and lose energy. The D layer's ability to absorb radio waves occasionally serves a beneficial purpose, e.g. it may decrease interference from other radio stations and increase the ratio of signal to noise of nearby stations using frequencies below 10 MHz. Thus, only the local signals may be received since the D layer absorbs the undesirable signals from distant stations.

In general, the D layer's significance stays in its function in controlling radio wave propagation, which has significant implications for several applications, including communication, navigation, and weather forecasting. For these applications to be optimized and improved, it is essential to comprehend the characteristics and behavior of this particular region.

1.2.3.3 E Layer

The UV light from the Sun is principally responsible for the formation of the ionosphere's E layer. Since the air density is lower and the ionization process is more effective at higher altitudes, the E layer is normally located between $90-120km$ above the Earth's surface. The ionization of neutrals in the atmosphere by solar radiation results in the creation of the E layer [16]. In particular, the UV radiation, ionize atomic oxygen (O) to generate O^+ ions, which then combine with neutral air molecules like nitrogen (N_2) and oxygen (O_2) to make molecular ions like NO^+ and O_2^+ [17]. The ionization process is finished when these molecule ions interact with free electrons to form more O^+ ions.

This particular ionospheric region is crucial for long-distance radio transmission, as it reflects waves with frequencies between 3 and 30 MHz, allowing radio communications over long distances with comparatively little power. Furthermore, this layer has significant real-world implications for navigation and communication.

Es Layer

This is also known as the sporadic E layer, as it develops in mid and higher latitudes during sporadic occurrences [18]. It differs from the conventional E layer in that it develops at a higher altitude and is more localized, generally manifesting as patches (or clouds) that can emerge and go within of minutes or hours. Solar radiations are main source of ionization here,thus at night the ionization reduces and this layer normally

vanishes. The Es layer can, however, develop inside the E layer in some circumstances due to areas of intense ionization. These spots can last for a few minutes to a few hours and rise up to $110km$. The E_s layer has a major impact on radio transmission, especially in the (very high frequency) VHF wave modes. It can cause radio signals to be refracted and hence allows for longer propagation lengths and the capacity to receive signals from far farther away than is typically feasible.

1.2.3.4 F Layer

The F layer, often referred to as the Appleton-Barnett layer, is the topmost layer of the ionosphere and is situated 200 to 400 kilometers above our Earth. Extreme solar UV and X-ray radiations causes neutral atoms and molecules, (including oxygen and nitrogen) to become photo-ionized. The F layer is further separated into the F_1 and $F2$ sub regions, which are identified by their different electron density profiles and refraction properties. While the F_2 layer is generated at an altitude of around 250 to $400km$, the F1 layer is formed in a range of 150 to $250km$ [19]. The F layer is also crucial to radio transmission because it enables long-distance radio communication.

The ionization of neutrals by solar radiation, results in the formation of the $F1$ layer. The ions and electrons can combine once more to form a layer of plasma that reflects radio waves up to around $10MHz$. In contrast, the F_2 layer is created when the Sun's intense UV radiation ionizes the molecules of atomic oxygen and nitrogen. Thus, the F2 layer may reflect HF$(10MHZ - 30MHZ)$ radio waves since it has a larger concentration of plasma species. This allows radio communication over extremely great distances. They are crucial for understanding the Earth's upper atmosphere and ionosphere as well as the transmission and reception of GPS signals.

1.3 Plasma density fluctuations in the ionosphere

Plasma density changes in the ionosphere due to several reasons, in the following we briefly describe some of the most important processes.

1.3.1 Solar activity

Solar activity is one of the main ragent that causes changes in plasma density in the ionosphere. Periodically, the Sun's radiative output changes, and during these times, the ionosphere gets exposed to a greater quantity of energy, causes an enhancement

of plasma density [20]. An opposite trend is true for low solar activity periods. Radio communications and other technologies that rely on the features of the ionospheric atmosphere may be significantly affected by this variation in plasma density.

1.3.2 Geomagnetic storms

Geomagnetic storms mainly affect the lower ionosphere, especially at high and middle-latitudes. At high latitudes, the disruption is immediate and strong, while at middle-latitudes, it has a long-lasting impact. Moreover the lower thermosphere is also significantly impacted by such storms [21]. In particular, the geomagnetic stroms have major effect the Earth's atmosphere where there is a high concentration of ions and free electrons [22]. During a geomagnetic storm, there is an increase in the flow of charged particles from the Sun, which can damage radio communications, harm satellite navigation systems, and disrupt the ionosphere [23].

1.4 Significance of ionospheric research

The radio wave communication system utilizes the radio wave to transmit information from one region to another. The radio wave communication system has numerous uses such as broad-casting two-wave communication, and global navigation. In short, radio wave communication plays a significant part in modern society and technology.

Plasma frequency is oscillation frequency in a fully ionized plasma. Plasma frequency depends on the square root of plasma density. With $m_e$is the mass of electron plasma frequency (f_p) can be written as

$$f_p = \sqrt{\frac{n_e e^2}{m_e \varepsilon_o}} \tag{1.1}$$

The process of transmitting and receiving radio waves strongly depends on the ionosphere. These wave can be refracted, reflected, or absorbed as they pass through the atmosphere and into the ionosphere during transmission [24]. The ionosphere's density, radio wave frequency, and angle of incidence are the possible factors that can affect the radio wave in the ionosphere. Different radio wave frequencies can be reflected by the ionosphere in different ways, e.g. those at lower frequencies, can be absorbed by the ionosphere, which can weaken the radio signal.

Critical frequency is the highest magnitude of frequency above which the frequency (f) the waves penetrate the ionosphere and below which the waves are reflected back from

the ionosphere.

where f_c is given by

$$f_c = 9\sqrt{n_{max}} \tag{1.2}$$

Here n_{max} is the maximum electron density.

If $f > f_c$ the incoming wave penetrates the layer and $f < f_c$ then incoming wave reflects. Hence, choosing the right frequency is essential for providing effective signal transmission [25]. The E layer can impact radio wave propagation for which lower usable frequency (LUF) are established in order to choose the best frequency. While frequencies below the maximum usable frequency (MUF) are reflected, frequencies beyond the MUF can go past the ionosphere and into space. We note that LUF is the lowest frequency that the D layer can totally absorb. Depending on the time of day, a different frequency may be appropriate, with lower frequencies being preferred at night and higher frequencies being appropriate during the day [26].

In general, radio waves over 30 MHz pass directly through the ionosphere and out into outer space rather than being reflected. The ionosphere, on the other hand, can get thicker and allow for the reflection of HF radio signals during times of powerful solar eruptions [27]. Radio waves with frequencies 30 MHz can be utilized to communicate between space and the Earth during these times of intense solar activity [28].

Various satellites are frequently used for transatlantic communication to over distant areas. For this, radio waves with frequencies higher than 30 MHz are used, and the satellites serve as reflectors. If the waves are within the coverage area of these artificial satellites, they are reflected to Earth when they arrive at them. However, these satellites have constrained coverage regions, are expensive, have a short lifespan of only approximately 25 years, and need regular maintenance. On the other hand, the ionosphere, surrounds the whole globe and acts as a natural satellite, reflects radio signals at frequencies below 30 MHz. As long as the Earth is in existence, the ionosphere will be used and will not require any upkeep or additional energy.

Navigation systems are also impacted by the ionosphere, especially those that depend on radio signals for precise location. Radio signals can be bent or refracted by the ionosphere, which results in longer trips through the atmosphere and false distance measurements as demonstrated in Fig.1.2.

Ionospheric delay is the term used to describe it's impact on navigation systems [29]. In particular radio transmissions experience this delay when they pass through the

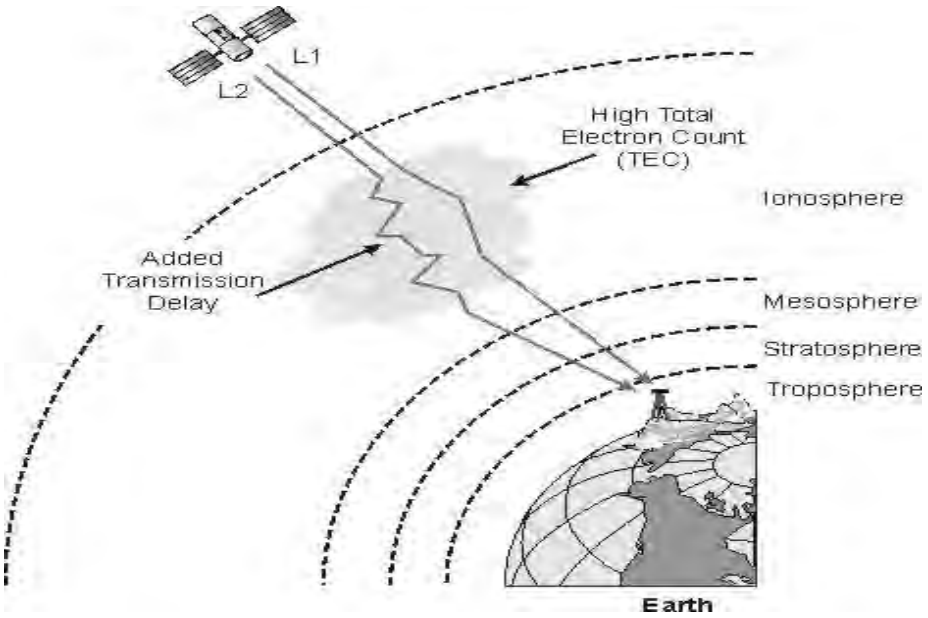

Figure 1.2: Schematics of the ionosphere effecting the GPS signals [31].

ionosphere, which slows down and extends the time it takes for the signal to arrive at the receiver. The delay depends on the signal's frequency, angle of incidence, and ionosphere density, among other things [30].

Our study centers on the low latitude region of the ionosphere. In the following section, we will explore the physics underlying the characteristics of the ionosphere at low latitudes.

1.5 Physics of low latitude ionosphere

The upper atmosphere of the Earth's surface, namely ionosphere, has an impact on radio wave propagation [32]. The thermosphere's day and night hemispheres receive different amounts of solar energy, which results in pressure gradients that give rise to a worldwide neutral wind system. This wind system helps in the distribution of energy and momentum both within and beyond the ionosphere. Within 60 degrees of latitude, the thermosphere's wind drives the electrodynamics of the system in the low-latitude ionosphere [33], supplying the mechanical energy required for global-scale dynamo. The ionospheric electrodynamic processes are highly variable in the low latitudes, an remain to be an active area of research for more than 50 years [34].

1.5.1 Ionospheric dynamo

The dynamo process, which describes a differential interaction of ions, electrons, and neutrals, produces electric fields in the ionosphere. A conductor traveling over magnetic lines of force causes an electromotive force (EMF), which is the fundamental working principle of a dynamo. The conducting ionosphere is moved across the Earth's magnetic field by the neutral winds, which induces EMFs and consequently electric fields. The current produced by the wind with velocity $(\vec{U})$ is identical to the current produced by an electric field with magnitude and direction $\vec{U} \times \vec{B}$ where $\vec{B}$ refers to the geomagnetic field. The major cause of the dynamo activity is the difference between the gyrofrequency and collision frequency of ions and electrons [35]. There are two primary categories of dynamos in the equatorial ionosphere: the E region dynamo dominates during the day, and the F region dynamo, which takes over at night. In the following section we describe the two dynamos in detail.

1.5.2 E region dynamo

Neutral winds have a significant impact on the electrodynamics of the E region; whereas the ion's motion is controlled by neutrals in this region, the electrons are magnetized. The high levels of Hall conductivity are primarily responsible for the E region's high conductivity throughout the day. The whole dayside ionosphere, where currents are generated by lower thermosphere tides, is an excellent electrical conductor. The differential heating of the atmosphere, results in the formation of winds at lower altitudes, electric currents are produced due to of the interaction between these winds and the ionosphere as they go higher. These currents are primarily produced by the E region dynamo, which is an essential component of the ionosphere's electrodynamics [36]. The E region of the ionosphere is influenced by a global tidal wind field, denoted as U(r, t). This wind field drives a global current system, which can be expressed mathematically as [37]

$$\vec{J}(r,t) = \sigma(r,t) \left[\vec{U}(r,t) \times \vec{B}\right] \tag{1.3}$$

Note that the conductivity and wind velocity depend on the location (r) and time (t). The electric current (J) in the ionosphere may not be divergence-free as a result of these oscillations, meaning it may include sources and sinks. An electric field is added to balance out the total current's non-zero divergence to produce a divergence-free current.

This leads to a more even and stable distribution of current throughout the ionosphere, i.e.

$$\vec{\nabla} \cdot \left[\sigma \left(\vec{E} + \vec{U}(r,t) \times \vec{B} \right) \right] = 0 \tag{1.4}$$

We can estimate that there will be a daily fluctuation in the electric field pattern at low latitudes. As a result, the electric field will display a diurnal pattern that varies throughout the day. While at higher latitudes, we may anticipate a mix of twice-daily and daily fluctuations in the electric field. Thus, a combination of diurnal (occurring once per day) and semi-diurnal (occurring twice per day) patterns will be visible in the electric field. The primary goal of these studies is to understand how tidal winds – also referred to as dynamo winds – vary with latitude and to investigate the physicsl mechanism by which these tidal winds produce electric fields in the ionosphere.

1.5.3 F region dynamo

The changing pressure in the thermosphere due to solar heating leads to horizontal winds, which move the charged particles in the F region. The particles, including ions and electrons, primarily drift along the Earth's magnetic field lines. Additionally, there is a slower sideways drift as caused by interactions with the neutral wind. This motion of ions creates an electric current in the mid-latitude F region. There is a significant electric current flow at night in the ionospheric F region, referred to as the "F layer dynamo current [38]."

When addressing diurnal phenomena in the ionosphere, it's crucial to be aware of the terminology differences. In the lower thermosphere (E layer), the vertical movement of the atmosphere is referred to as a "diurnal tide" whereas in the higher thermosphere (F region), called a "diurnal wind". It is proposed that the mesosphere's heating causes the diurnal tide in the E layer. This heating results from the ozone layer's absorption of solar UV light. Vertical oscillations and the production of tidal winds are caused by the energy that is absorbed in the ozone layer and propagates higher. The diurnal winds in the F region, on the other hand, are mostly caused by heating of the F region itself. Extreme UV light from the Sun is the main cause of this heating since it not only causes ionization but also creates thermal energy. This thermal energy causes horizontal winds to form in the upper thermosphere, which affects the dynamics of the F region. The current in the F region has the same ability to induce an electric field polarization as the current in the E region. However, the existence of strongly conducting E layers coupled

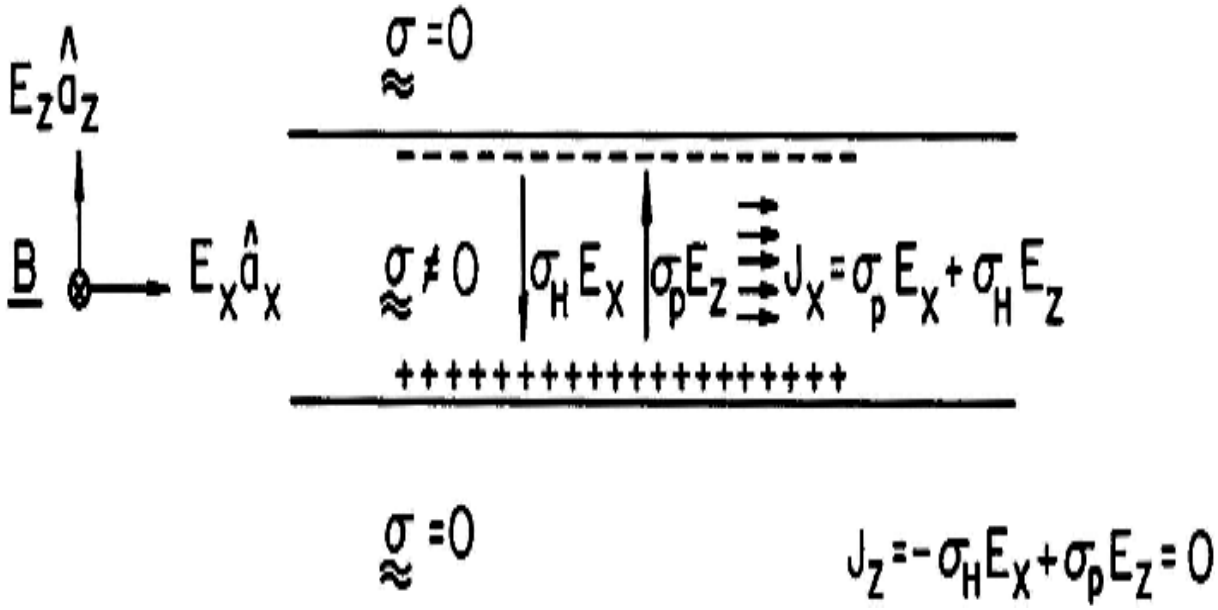

Figure 1.3: Electrodynamics of the equatorial F region in, which the density and the conductivity profiles are modeled with a slab geometry [Kelley, 2009].

by magnetic field lines in the F region effectively neutralizes this polarization electric field. polarization charges can build up at night because the E layer's conductivity is lower, which weakens the shorting out of the action [39].

Figure 1.3 depicts a simplified representation of the equatorial F layer in a slab geometry, assuming that the conductivity is zero both below and above the slab. Additionally, a constant eastward zonal wind with a velocity of u is considered, for which the current induced by the motion of neutral winds is described as

$$\vec{J} = \sigma \left(\vec{u} \times \vec{B} \right) \tag{1.5}$$

The current in the F layer is directed vertically in the z-direction, as seen in Fig.1.3. However, charges build up at the borders because the current is not divergence-free. A vertically downward polarization field is created as a result of this charge buildup and is represented as

$$\vec{E_z} = -u\vec{B} \tag{1.6}$$

Due to the interaction between the vertical polarization field and the horizontal geomagnetic field, the plasma within the F layer experiences an eastward $\vec{E} \times \vec{B}$ drift. This drift velocity is typically close to the velocity of the neutral wind. However, it is important to note that these observations are based on the assumption that the conductivity

of the E region, which lies below the F layer, becomes negligible after sunset. In reality, the conductivity of the E region usually has a small, finite value. When the conducting E layer is considered in the model, the expression for vertical electric field is given by

$$E_z(z) = \frac{-u(z)B\sigma_p^F(z)}{\sigma_p^F(z) + \sigma_p^E(z)} \tag{1.7}$$

The integrated conductivities along the magnetic field lines for the E and F regions of the ionosphere, respectively, are represented by σ_P^E and σ_P^F in the above equation. The vertical electric field is largely affected by the neutral wind's speed at night because the field line integrated conductivity of the E zone is comparatively low. However, during the daylight, $\sigma_p^E \geq \sigma_P^F$, creating a small vertical electric field. An important part in creating electric fields is played by the unique arrangement of the Earth's magnetic field at the equator in conjunction with the ionosphere's wind patterns. In this regard, the equatorial electrojet (EEJ), is one of the phenomena caused by these electric fields, is one of these phenomena. The term EE describes the strong eastward electric current present in the ionosphere close to the magnetic equator.

1.6 Ionosphere Currents

In the E-region of the atmosphere, ions, and to a lesser extent, electrons, exhibit coupling with the neutral constituents, aligning with their dynamic behavior. Atmospheric winds and tidal oscillations impart forces on the E-region ion component, compelling movement along magnetic field lines, while electrons exhibit a relatively slower motion perpendicular to both the field and the neutral wind. The differential motion gives rise to an electric current, and the spatial separation of charge engenders an electric field, subsequently exerting an impact on the current.

For mid and low latitudes, the primary driving force for the current is the $V \times B$ field induced by ion motion across the magnetic field. We will delve into specific currents in the following sections.

1.6.1 Sq Current

The most important dynamo effect at mid-latitude is the daily variation of atmospheric motion caused by the tides of atmosphere. The tides with the lowest and largest amplitudes are the diurnal and semi-diurnal oscillations which are excited by the solar

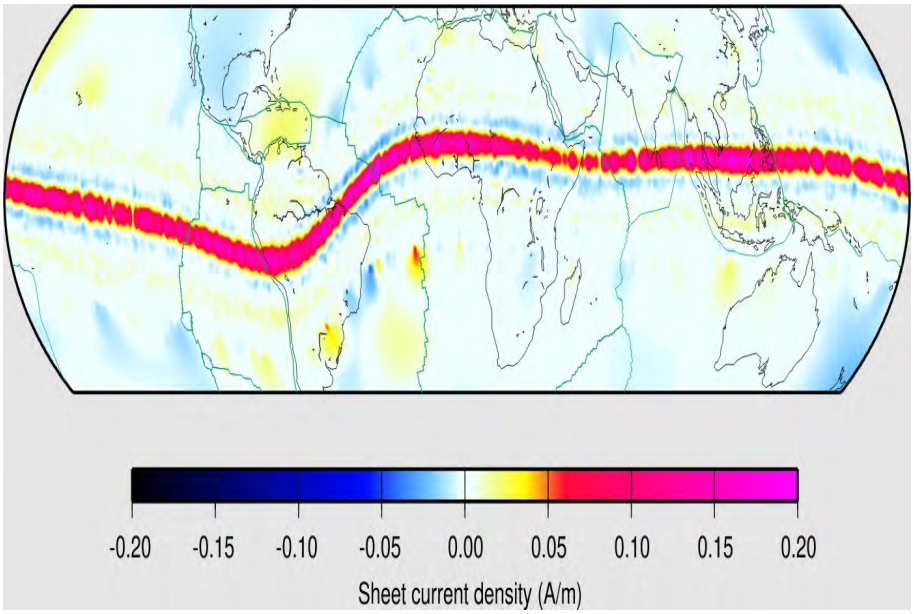

Figure 1.4: The depiction of EEJ dansity as obtained by the CHAMP satellite, during its 2600 passes over magnetic equator (11:00 and 13:00 local time). `geomag.org`].

radiation heating of the atmosphere. The current system created by this tidal motion of the atmosphere is called solar quiet or Sq current.

1.6.2 Equatorial electrojet (EEJ)

Around the magnetic equator, a powerful current namely EEJ travels in an east-west direction. It ranges from a height of around 100 to 110 km and covers about 3 degrees of latitude on either side of the equator. The E region dynamo in the ionosphere produces an eastward electric field that predominantly powers the EEJ. It is crucial to understand that the EEJ differs from the typical Sq current, and is created as a result of the unique arrangement of the terrestrial magnetic field at the equator. The discovery of the EEJ was made possible by an unusual finding in the daily change of the horizontal component (H) of the magnetic field. When compared to other latitudes, the H-component at the magnetic equator showed an unexpected enhancement [40]. Figure 1.4, shows the daily range of the horizontal component of the Earth's magnetic field at various latitudes. The peak at the dip equator can be seen to be of a substantial magnitude, EEJ presence has been suggested as the cause of this particular impact [41].

Numerous techniques, including ground-based magnetometer readings, rocket tests, and radar studies, have been used to investigate EEJ and its effect on ionosphere dynamics [42]. Researchers have made tremendous progress in understanding the complex relationship between the EEJ current and its impacts on the ionosphere by inte-

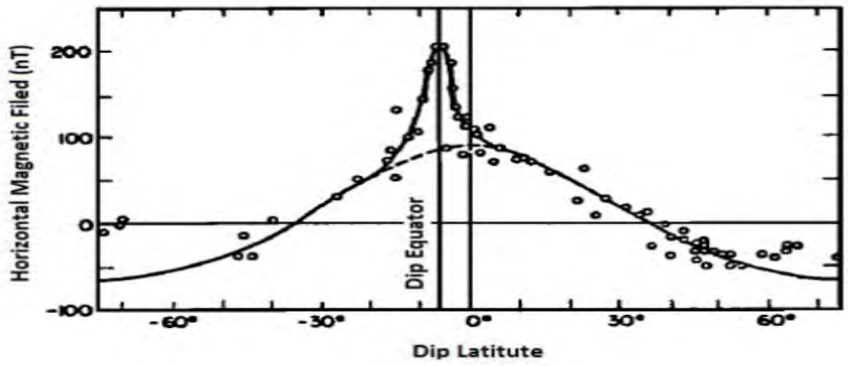

Figure 1.5: The presence of an equatorial noontime enhancement in the H-component of Earth's magnetic field serves as a distinct indicator of the EEJ. [Onwumechili, 1967].

grating data from many sources [43].

In the dynamo region of the ionosphere near the dip-equator, the horizontal northward geomagnetic field $\overrightarrow{B}$ and zonal electric field $\overrightarrow{E}_y$, produce an eastward Pedersen current $\overrightarrow{J}_{p1}$ (Eq. (16)), and a vertical downward Hall current $\overrightarrow{J}_{H1}$ (Eq. (2)) associated with electrons upward vertical $\overrightarrow{E} \times \overrightarrow{B}$ drift shown in Fig. 1.6.

In mathematical terms, we can express the components of current density in the following form [1].

$$\overrightarrow{J_{p1}} = \sigma_p \overrightarrow{E_y} \tag{1.8}$$

$$\overrightarrow{J}_{H1} = -\sigma_H \left(\frac{\overrightarrow{E_y} \times \overrightarrow{B}}{B}\right) \tag{1.9}$$

σ_p and σ_H are respectively Pedersen and Hall conductivities.

On one hand, as ions $\overrightarrow{E} \times \overrightarrow{B}$ drift is impeded in the E-region due to collisions with neutral particles while electrons are relatively free to move, the resulting charge separation gives rise to an upward vertical polarization electric field $\overrightarrow{E_p}$. On the other hand, $\overrightarrow{E_p}$ gives rise to an upward vertical Pedersen current $\overrightarrow{J_{p2}}$.

$$\overrightarrow{J_{p2}} = \sigma p \overrightarrow{E_p} \tag{1.10}$$

When the polarization process is complete, the upward vertical Pedersen current $\overrightarrow{J_{p2}}$ counter-balances the downward Hall current $\overrightarrow{J_{H1}}$.

$$\overrightarrow{J_z} = \overrightarrow{J_{H1}} + \overrightarrow{J_{p2}} \tag{1.11}$$

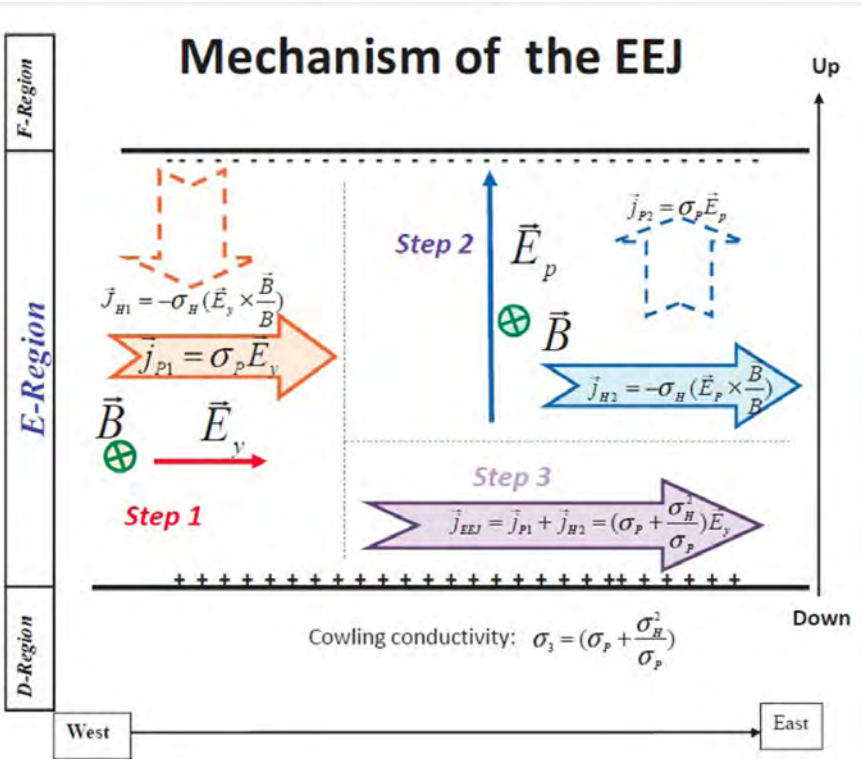

Figure 1.6: The representation of a slab geometry depicting a model from EEJ [1].

$$\overrightarrow{J_z} = \sigma p \overrightarrow{E_p} - \sigma_H (\frac{\overrightarrow{E_y} \times \overrightarrow{B}}{B}) = 0 \tag{1.12}$$

And the $\overrightarrow{E}_p \times \overrightarrow{B}$ westward electron drift gives rise to an intense eastward Hall current $\overrightarrow{J_{H2}}$.

$$\overrightarrow{J_{H2}} = -\sigma_H (\frac{\overrightarrow{E_p} \times \overrightarrow{B}}{B}) \tag{1.13}$$

so,

$$\overrightarrow{J}_{EEJ} = \overrightarrow{J_{H2}} + \overrightarrow{J_{p1}} \tag{1.14}$$

$$\overrightarrow{J}_{EEJ} = \sigma_p \overrightarrow{E_y} + (-\sigma_p (\frac{\overrightarrow{E_p} \times \overrightarrow{B}}{B}) \tag{1.15}$$

From Eq. (12) the vertical polarization electric field can be expressed by Eq. (16)

$$\overrightarrow{E}_p = \frac{\sigma_H}{\sigma_P} (\frac{\overrightarrow{E_y} \times \overrightarrow{B}}{B}) \tag{1.16}$$

Replacing E_p in Eq. (2)5, the equatorial electrojet net current density $\overrightarrow{J}_{EEJ}$ can be

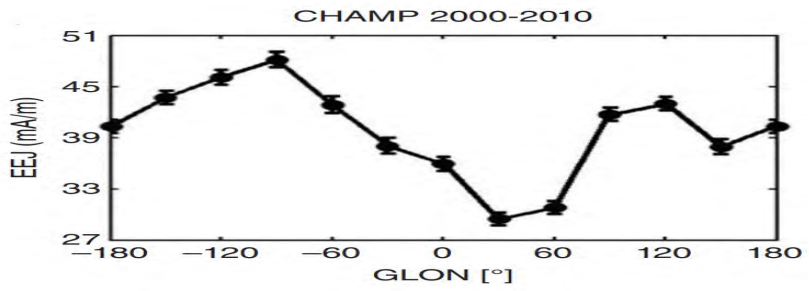

Figure 1.7: The longitidinal variation of averaged EEJ [2].

expressed as:

$\overrightarrow{J}_{EEJ} = (\sigma_p + \frac{\sigma_H^2}{\sigma_p})\overrightarrow{E}_y$

Where $\sigma_C = (\sigma_p + \frac{\sigma_H^2}{\sigma_p})$ is the net eastward conductivity known as "Cowling conductivity" [44]. Whereas in the E region $(\sigma_H \gg \sigma_P)$. Furthermore, Cowling's conductivity is significantly higher than the of Hall and Pedersen counterparts. The equatorial electrojet current, which flows in an easterly direction, is produced mailny by the higher Cowling conductivity.

1.6.2.1 Longitudinal variation of EEJ

The longitudinal variation refers to the changes observed as one moves along the Earth's longitudinal axis. It is characterized by variations in the intensity and location of the EEJ current system at different longitudes. Understanding the longitudinal variation is essential for comprehending the dynamics and behavior of the EEJ. The asymmetry in the geomagnetic field configuration and its interaction with ionospheric plasma currents are the main factors affecting the longitudinal fluctuation of the EEJ. Near the dip equator, where the geomagnetic field is almost level and perpendicular to the surface, the EEJ is most noticeable. The inclination and strength of the magnetic field fluctuate as we go away from the dip equator down the longitudinal axis, causing variations in the intensity and position of the EEJ.

The distribution of the EEJ peak current density's yearly averaged is presented in Fig. 1.7. While a secondary peak may be observed in eastern Asia, the largest amplitudes are seen close to Huancayo in south America. However, across east Africa and some regions of India, the lowest EEJ amplitudes are frequently observed [45].

Ionospheric conductivity has probably increased, which may be inferred from the EEJ's large amplitudes across south America. As a result of the reduced magnetic field, this is particularly obvious there. The magnitude of the magnetic field has an inverse connection with both the Hall and Pedersen conductivities [46].

The longitudinal variation in the ionospheric conductivity is one of its key features. The ionosphere's conductivity changes with latitude, altitude, and local time. These differences have an impact on the EEJ's E field associated with, which in turn affects the current system's position and strength. The longitudinal variation enables researchers to look at how variations in conductivity along various longitudes affect EEJ. The zonal winds and temperature gradients in the atmosphere have a strong influence on the longitudinal fluctuation of the EEJ. The ionosphere's zonal winds have a substantial impact on the plasma drift, that affects the EEJ.

1.6.2.2 Seasonal variation of the EEJ

Seasonal fluctuations affect several variables, such as variations in the geomagnetic field, ionospheric conditions, and seasonal solar activity. The EEJ typically peaks around the equinoxes which take place in March and September. This is because the duration of the day and night is almost equal during these periods. The equinoxes are linked to increased ionization in the ionosphere and higher solar heating. Strong sunshine and longer daylight hours help create a bigger eastward electric field, which in turn generates a higher EEJ current. In contrast, the EEJ is often weaker around the solstices (in June and December). This is because different daylight duration's and unequal heating across the hemispheres are caused by the Earth's tilt about the Sun.

Figure1.8 shows that the predominant currents typically move westward in the morning at 06 LT (local time). However, eastward currents take over in the rest of the day only about an hour later. This points to a change from westward to eastward in the large-scale background electric field at 07 LT. In the hours that follow, the current's intensity quickly increases until it reaches its greatest value about 11 LT. The current density monotonically drops throughout the day and ultimately disappears at about 18 LT.

The peak noontime current is greatest around the equinoxes and is at its lowest throughout the summer in the northern hemisphere. Additionally, the diurnal evolution depicts a slight delay at the June solstice.

When studying the average amplitude variation across the months of a year, as indicated in Fig.1.9 , the seasonal fluctuation of the EEJ, as shown in Fig.1.8, becomes more apparent. The EEJs that are strongest occur in March, April and October, i.e., during the equinoxes when the large-scale tidal breezes are at their highest. The EEJ amplitudes, on the other hand, significantly decline in July, reaching only roughly two-thirds of the values seen during the equinox months.

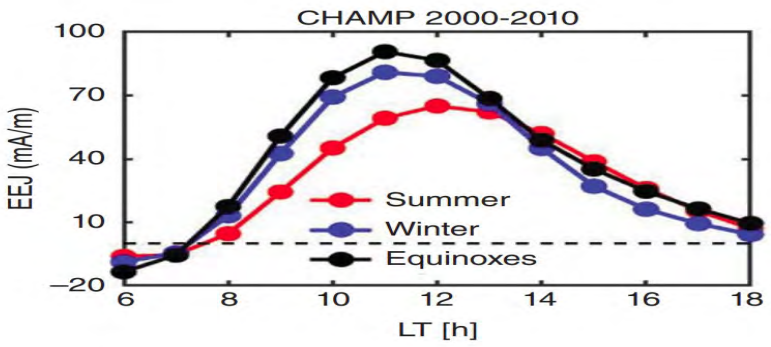

Figure 1.8: The daily average variation of the EEJ peak current density integrated over height. It focuses on the CHAMP mission period and examines three specific seasons; [Fejer 2021].

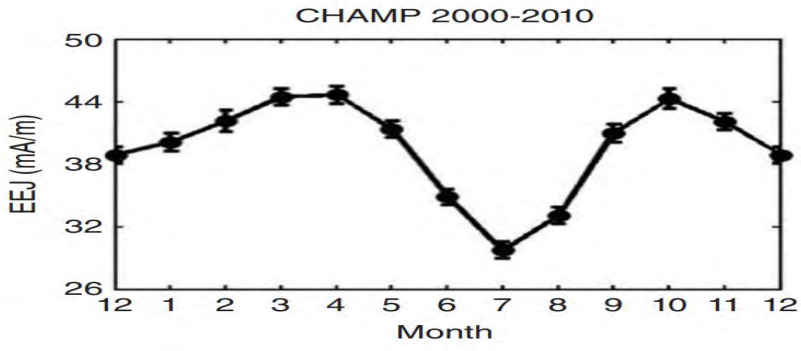

Figure 1.9: Annual variation of EEJ current density [Fejer 2021].

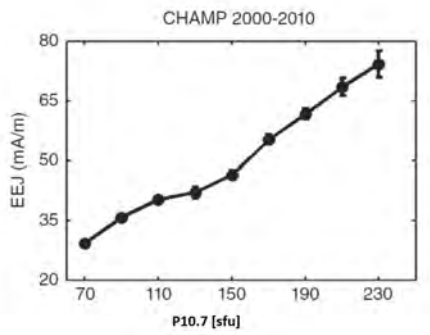

Figure 1.10: Variations in EEJ with the solar flux index P10.7 [2].

1.6.2.3 Dependence of EEJ on solar flux

The EEJ also shows a dependency on solar flux, which is the quantity of solar radiation or energy received from the Sun. The ionization and conductivity of the upper atmosphere of the Earth are influenced by solar flux, which is a key factor in ionospheric processes.

Increasing ionization in the ionosphere can result from higher solar flux levels. The ionospheric layer, including the region where that EEJ flows, becomes more conductive as a result of the increased ionization. As a result, the EEJ tends to be stronger during times of increased solar radiation.

It is known that years of high solar activity, or solar maximum years, are characterized by an increase in the amplitude of the EEJ [47]. The CHAMP satellite mission's observations have confirmed this connection [48]. This relationship is illustrated in Fig.1.10, which depicts a continuous rise in current density as the solar flux index, which is represented by the smoothed $P10.7$ solar flux data, rises. As the solar flux levels increase from 70 to 230 solar flux units (sfu), the EEJ's amplitude becomes more than two fold.

1.6.2.4 Dependence on geomagnetic activity

The EEJ currents often show larger amplitudes during calm geomagnetic periods. However, the perturbed magnetic field might interfere with the electric currents in the EEJ when magnetic activity rises, i.e., during geomagnetic substorms. The EEJ currents' strength may decline as a result of this disturbance [49].

It is clear from Fig. 1.11 that during low and moderate magnetic activity, the average current density of the EEJ is rather steady. The mean amplitude of the EEJ, however, tends to decline and, in some instances, even turn negative during periods of intense magnetic activity.

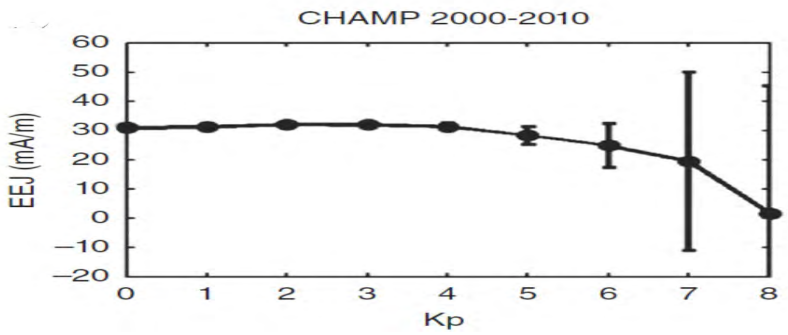

Figure 1.11: Dependence of EEJ on the magnetic activity [Fejer 2021].

The huge error bars show that the EEJ signature is very variable, especially during periods of activity. The disturbance dynamo wind, which reaches its peak about three hours following a significant spike in magnetic activity, is principally responsible for the lower amplitude during periods of high magnetic activity [50].

The atmospheric winds produced in reaction to changes in the geomagnetic field are referred to as the disturbance dynamo wind. These winds, which are caused by the magnetic field and ionosphere interacting, have a big impact on how the EEJ behaves. The disturbance dynamo wind can offset or reduce the EEJ currents at times of increased magnetic activity, causinga decrease in the amplitude of EEJ.

1.7 Counter Equatorial electrojet(CEEJ)

The behavior of the EEJ changes greatly from day to day [Forbes, 1981]. During a low geomagnetic activity, there are times when the EEJ weakens rapidly, transitioning from the usual positive values to negative values. This unusual condition lasts for only few (2-3) hours before returning to normal. This is known as “counter-equatorial electric current (CEEJ)” because the direction of the current reverses inversely to the normal direction of the equatorial electrojet. The CEEJ occurs mostly in the local afternoon and seldonly in the morning. It should be noted that in times of magnetic disturbances, this phenomenon cannot be CEEJ. While the exact physics of CEEJ formation is not fully understood, two theories are attempting to explain it. One theory states that there may be a reversal of the vertical polarity of the electric field in the EEJ range due to possible local interactions with winds of different heights . The second theory suggests that the zonal (east-west) electric field reversal influenced by global tidal wind patterns could contribute to the occurrence of CEEJ. While the second theory has proven comparatively more successful than the first, a full understanding of the physical mechanism behind

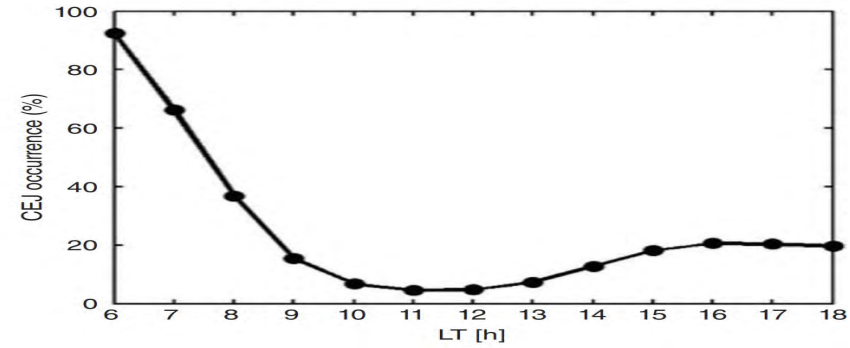

Figure 1.12: Dependence of counter electrojet on local time [Fejer 2021] .

CEJS is still the subject of ongoing research [51]. The counter-electrojet does not occur randomly but shows clear daily, longitudinal, and seasonal fluctuations. In the morning between $06:00$ and $07:00$ local time (LT), it can be observed about 90% of the time at all longitudes, as shown in Fig.1.12. This observation is consistent with earlier measurement of magnetic field by Cohen and Achache (1990) the Magsat satellite. The high frequency in the morning is due to the nighttime electric field prevailing from the west. In the following hours, however, the east-directed electric field dominates, causing the counter electromagnetic dip to drop to about 4% around noon. In the evening, the value gradually approaches an average of 18%.

1.8 Aims and Objective

This research aims to deepen our understanding of the EEJ within the Earth's ionosphere. The investigation involves a comprehensive exploration of the EEJ's diurnal behavior, with a specific focus on discerning how its intensity and dynamics undergo variations over a 24-hour period. Additionally, the study extends to analyzing seasonal changes in the EEJ. Another crucial facet of the research involves delving into the relationship between sunspot numbers, indicative of solar activity, and the observed diurnal and seasonal variations in the EEJ. By conducting this analysis, the research aims to unravel the ways in which solar variability influences the behavior of the EEJ. In combine these aspects, the study seek to contribute valuable insights to the broader fields of ionospheric physics, space weather forecasting, and technological applications that rely on a nuanced understanding of the EEJ's behavior.

1.9 Thesis Layout Summery

In this dissertation, our focus has been a comprehensive exploration of the EEJ and its distinct features, which include changes throughout different seasons and twilight periods, as well as its correlation with the SSN. Our study is meticulously organized, beginning with foundational concepts and a thorough analysis of the research problem, building upon historical research in this field. This initial exploration serves to establish a strong understanding of fundamental concepts within our research area.

We then delve into explaining the specifics of our dataset and the methodologies employed throughout this study. The dataset, acquired from ground-based magnetic observatories connected to the "INTERMAGNET" resource, spans a continuous five-year period from 2018 to 2022. Our analysis of the EEJ involves using an off-separation method, assessing the strength of the EEJ index. In this method, data from observatories off the equator are distinguished from those at equatorial locations. To understand the impact of EEJ on the ionosphere, we examine changes in the magnetic field.

Given the substantial influence of the ionosphere on radio wave transmission, the density of the EEJ becomes crucial for effective communication. Consequently, variations in the EEJ hold considerable importance for everyday communications. Our investigation includes analyzing fluctuations in EEJ across different seasons and times of day, as well as exploring the influence of the Solar Sunspot Number on these EEJ variations.

Moreover, Chapter 2 delves into the approach we employed for our analysis, exploring the intricacies of the dataset and the methodology employed in calculating the Equatorial Electrojet (EEJ). Moving on to Chapter 3, we will present the outcomes of our study, encompassing the annual, seasonal, and diurnal fluctuations of the EEJ. Additionally, we will examine the relationship between EEJ and sunspot numbers in this chapter. Subsequently, Chapter 4 will be dedicated to a comprehensive discussion of these findings. Finally, Chapter 5 will encapsulate our analysis in a succinct summary.

Chapter 2

Data sets and Methodology

2.1 Intermagnet

In the 19th century, the studies by Carl Friedrich Gauss and Alexander von Humboldt had a significant impact on the creation of the first magnetic observatory [52]. Since then the magnetic measurements have advanced significantly over time. Readings from magnetic survey equipment were first obtained visually, but they have since evolved to involve automatic photographic measuring and recent electronic acquisition. There are currently more than 170 magnetic observatories in operation around the globe. Out of them, about 120 centers routinely create and distribute digital data, while the other centers either rely on antiquated analogue systems or submit their data after measurements with a large delay[52].

The global distribution of digital data is facilitated by the INTERMAGNET organization [53], which is represented by the network of geomagnetic observatories. The INTERMAGNET was founded as a result of talks that took place at the Nordic comparison meeting in Chambon La Foret, France, in May 1987 and the workshop on magnetic observatory instruments in Ottawa, Canada, in August 1986. These incidents prepared a way for the creation of INTERMAGNET [53]. The data collected through magnetic field recordings is made readily available for use and is commonly referred to as reported data [53].The initial step in processing the data involves removing any contamination caused by errors from instruments or human actions to obtain the adjusted data The baseline is then created by combining this corrected data with a set of reliable absolute field measurements. The resulting dataset, which exhibits the absolute values of the magnetic field at the site, is known as conclusive data. Observatories are encouraged to

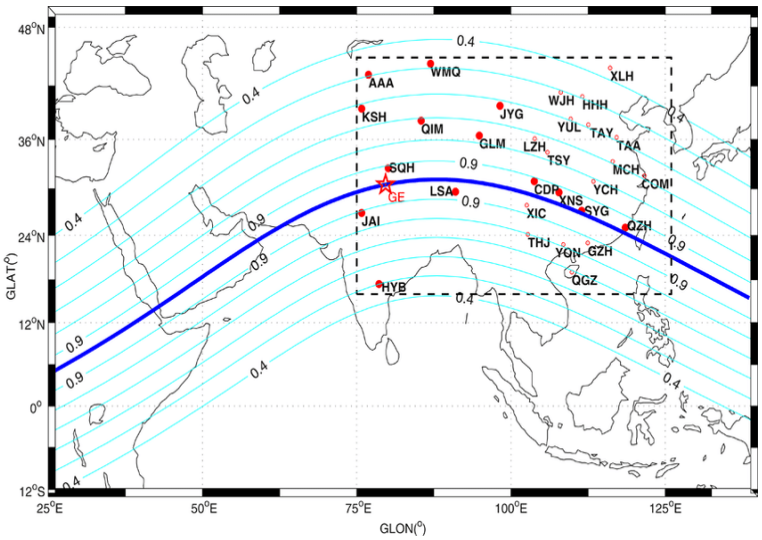

Figure 2.1: Cartographic overview of geomagnetic observatories [3].

produce data with resolutions as low as one minute or even one second, recording variations in the magnetic field over brief time intervals. This high-resolution data, shown as (H, D, Z) or (X, Y, Z) components, can be uploaded to the INTERMAGNET database. The brief distribution map of various geomagnetic observatories is depicted in Fig. 2.1.

China runs a vast network of geomagnetic observatories in addition to INTERMAGNET. These observatories are a part of the china geomagnetic network center (GNC), which is a division of the China earthquake administration's institute of geophysics. These observatories are located all over the nation, and the GNC is in charge of managing and supervising their operations.

2.2 Geomagnetic observatories

Permanent monitoring stations known as magnetic observatories are used to detect the geomagnetic field over time intervals ranging from seconds to decades and even longer. These observatories require stable surroundings that last for a long period of time without experiencing any substantial interference from human activities or cultural influences that could affect the magnetic field readings. They were first created in the early 19th century as a result of the influence and concepts advanced by Alexander von Humboldt and Carl Friedrich Gauss [54]. Magnetic measurement methods have advanced significantly over time. The method was developed from straightforward magnetic survey equipment visual readings, including automatic photographic measuring and contemporary electronic acquisition techniques. Observatories are continually upgraded to collect data that adhere to more stringent criteria to satisfy the expanding expecta-

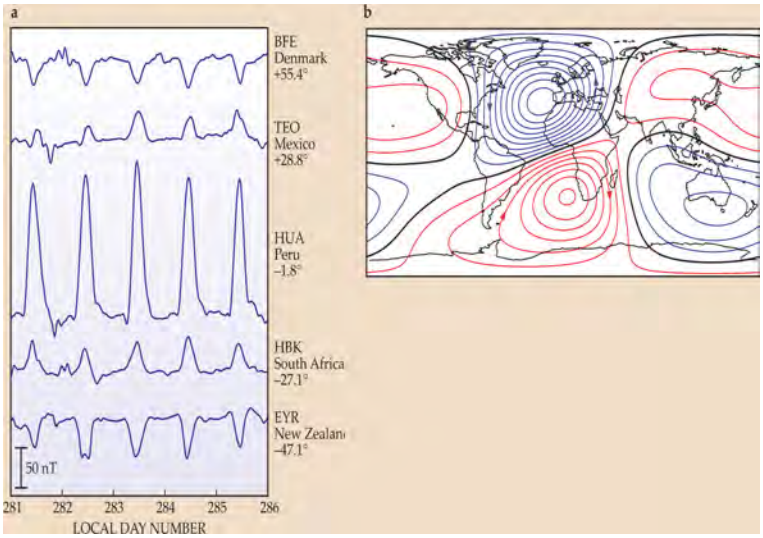

Figure 2.2: Readings of magnetograms during quiet times. (a) Temporal variation of horizontal intensity (H) across five observatories: 8-12 october 2003. (b) Ionospheric electric current mapping utilizing observatory data to capture quiet-time variation [56] .

tions of the scientific community. Higher acquisition frequencies will be attained with the help of these modifications, enabling more accurate and thorough measurements. Additionally, there is a focus on real-time data dissemination, guaranteeing that the scientific community may quickly access and analyze the information [55]. When we acknowledge the interconnection of the geomagnetic field across Earth and its surroundings, we may better comprehend the diverse applications of data collected from magnetic observatories. Electric currents create magnetic fields above and below us, which come together to form the overall geomagnetic field measured at observatories on the Earth's surface. This complicated field arises from various subtle physical occurrences in multiple geophysical domains, giving rise to a wide range of time-dependent behaviours.

It lies beyond the Earth's surface where the magnetic field weaves its course. Based on variables including height, latitude, time of day, season, and solar cycle phase, the degree of ionization changes. The motion induction method of producing electric currents is sustained in the altitude range of around 90-300 km by the interaction of winds brought on by temperature changes between day and night as well as tides influenced by the gravitational pull of the Moon and Sun. The electric currents of the ionospheric dynamo give observatory magnetograms a characteristic diurnal variation during quiet periods, when the magnetic field is comparatively undisturbed by solar activity, as seen in Fig. 2.2 (a).

Extended time series can be subjected to a thorough Fourier analysis to identify specific frequencies that correspond to related modulations driven by the solar cycle, Earth's

orbit around the Sun, the Moon's orbit around the Earth, and Earth's rotation. It is possible to trace the ionospheric currents related to these frequencies by using Ampere's equation. Figure 2.2 (b) shows that the two current gyros on Earth's dayside dominate the current system during times of quietness. The daily change in the magnetic field that is visible during quiet times is caused by Earth's rotation inside this current system. The daily variation in the magnetogram seen at Huancayo, Peru, is clearly shown in Fig. 2.2 (a). The Huancayo observatory was established by the Carnegie Institution of Washington in the 1920s, shortly after the first detection of this fluctuation. The ionosphere's anisotropic electrical conductivity is thought to be the cause of the observed variance. The interaction of the horizontal ambient magnetic field and the vertical electrical field – produced by charge separation across the ionosphere – on the dayside of the Earth, within a narrow band about 5 degrees wide near the magnetic equator, facilitates the east-west movement of charge carriers. This causes a concentrated flow of daylight electric current towards the east and causes the diurnal magnetic variation at observatories like Huancayo and Tatuoca, which are close to the magnetic equator, to be amplified in a way that can be seen.

2.2.1 Observatories utilized in our study

We have used the data from two observatories, namelt TTB (close to equator) and KOU (closest off-equatorial observatory to TTB).

The Tatuoca magnetic observatory, identified by the IAGA code TTB, boasts a rich history dating back to 1933 when a temporary magnetic observatory was established on Tatuoca Island [57]. The observatory's site was chosen on purpose to be in areas with low magnetic latitudes from the beginning [57]. Tatuoca's permanent magnetic observatory, with an inclination of 18.18 degrees measured [58], was built in 1954. Notably, the equator passed the observatory in March 2013 as it slowly moved northward over time. The details about the observatory are presented in tab. 2.1.

The KOU observatory at Kourou, French Guiana, is the closest neighbor to Tatuoca and is located about 700 km to the north and 400 km to the west of Tatuoca. The Institute de physique du globe de paris (IPGP) oversaw the construction of the KOU observatory in 1995. The magnetic readings made at Tatuoca are compared to and referenced against this observatory. To gain a better understanding of the regional fluctuations and peculiarities of the Earth's magnetic field in both equatorial and off-equatorial regions, the KOU observatory was strategically positioned relative to Tatuoca. The most relevant

Observatory	Geographic Latitude	Geographic Longitude	Geomagnetic latitude	Geomagnetic longitude
TTB	$-1.205°N$	$311.487°E$	$1.57S$	$24.05E$
KOU	$5.209°N$	$307.267°E$	$13.99°N$	$20.49°E$

Table 2.1: Details of the observatories used for our study [4, 5].

information and specifications regarding the observatory are presented in a tab. 2.1.

2.3 Calculation of EEJ

In this thesis, the off-equatorial subtraction method [59] is used to analyze and compute the EEJ. This technique is used to separate the magnetic signal uniquely related to the EEJ from other magnetic variations seen at off-equatorial geomagnetic observatories. For that the magnetic field measurements are gathered from equatorial and off-equatorial observatories and used to calculate the EEJ. To effectively collect the powerful eastward currents of the EEJ, the equatorial observatories are placed strategically close to the magnetic equator. The off-equatorial observatories are situated some distance from the magnetic equator, are subject to diverse magnetic forces. We utilized a dataset spanning five years, from 2018 to 2022, to investigate quiet conditions (Kp<3) in our study.

The magnetic field data obtained from the off-equatorial observatories are subtracted from the corresponding values at the equatorial observatories using the off-equatorial subtraction method (OSM). This subtraction procedure successfully eliminates magnetic changes as caused by solar quiet (SQ) and magnetospheric ring currents, which are not directly related to the EEJ. The difference that results, often known as the residual values, represents the magnetic signal that is mostly assigned to the EEJ. The behavior, properties, and temporal fluctuations of the EEJ currents in the equatorial ionosphere are clearly understood because of these isolated magnetic variations. It is significant to note that the OSM is the main strategy used in this thesis to determine the EEJ. The EEJ's contribution to the equatorial ionosphere can be determined by correctly using this procedure and examining the isolated magnetic signal.

The baseline value was determined by taking the average of night time magnetic field strength. The magnetic fields due to sources in space are obtained by subtracting the baseline from each magnetic measurements of the magnetometer at the equator and off the equator are given respectively by

$$\Delta H_{equ} = H_{equ} - H_{b(equ)} \tag{2.1}$$

$$\Delta H_{non-equ} = H_{non-equ} - H_{b(non-equ)} \tag{2.2}$$

where ΔH_{equ} and $\Delta H_{non-equ}$ stands for the total external magnetic field sources on and off the magnetic equator respectively. $H_{b(equ)}$ and $Hb_{(non-equ)}$are nighttime base line magnetic field measurements on and off the magnetic equator respectively. B-field from EEJ can be determined by removing the ring current and global Sq dynamo contribution to the H-component of the magnetic field recorded by magnetometer at the magnetic equator. This is done by subtracting the total external magnetic field sources recorded off the magnetic equator ($\Delta Hnon{-}equ$) from sources recorded on the magnetic equator ($\Delta Hequ$) assuming the effect of these currents at and off the equator. The EEJ value can be determined by subtracting the magnetic current at the equator from the magnetic current measured off the equator as given fallows.

$$\Delta H_{eej} = \Delta H_{equ} - \Delta H_{(non-equ)} \tag{2.3}$$

The EEJ value is determined in graph 2.3 using the OSM. Using data from both the off-equatorial observatory, KOU, which is positioned at a somewhat greater distance from the magnetic equator and the equatorial observatory, TTB, we can isolate the unique signal associated with the EEJ. For that we focus on the data for the month of January in this graph. TTB records a wide variety of signals because of its location closer to the magnetic equator. As an off-equatorial observatory, KOU, on the other hand, records magnetic alterations that are impacted by several variables. We only use information from quiet days to calculate the EEJ, and eliminate the other data by writing our MATLAB program.

It is worth mentioning that the TTB observatory is currently under the full influence of the EEJ, the KOU observatory, in contrast, is situated far from the magnetic equator, allowing it to record a variety of magnetic signals. Therefore, the magnetic signal related to the EEJ can be isolated by subtracting the magnetic data collected at the KOU observatory from the data obtained at the TTB observatory as demonstrated by Fig. 2.4. This procedure makes it easier to analyze separately the magnetic effects associated with the magnetospheric ring currents and SQ currents provide [60].

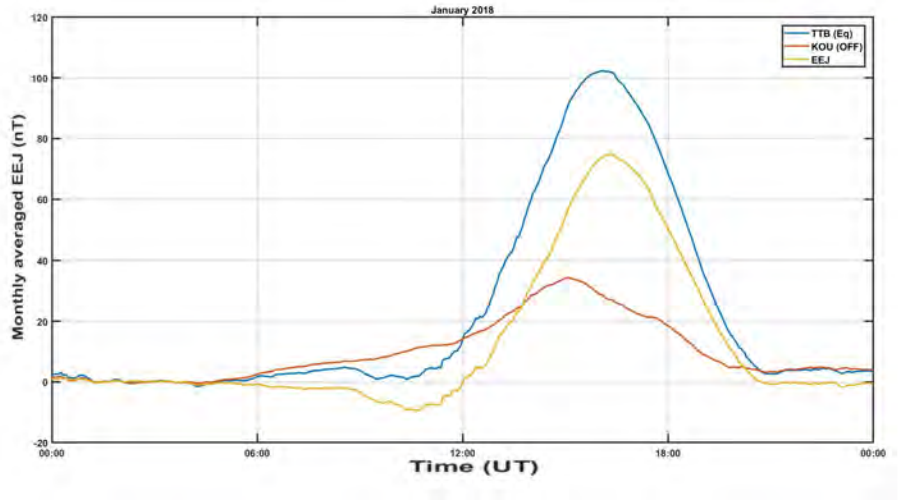

Figure 2.3: Calculation of EEJ through TTB(eq) and KOU(off-eq) observatories.

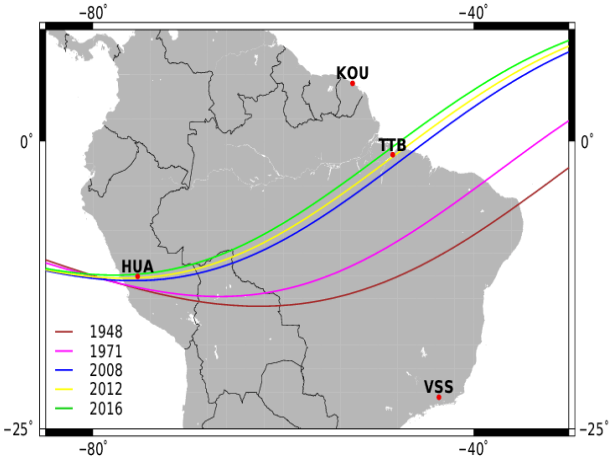

Figure 2.4: The Tatuoca (TTB) observatory's exact location is shown in the figure, along with other INTERMAGNET observatories in the vicinity, including Kourou (KOU), among others. Additionally, the International Geomagnetic Reference Field (IGRF) positions the geomagnetic equator in the picture for various years from 1948 to 2016. The geomagnetic equator's location and any variations over time are shown visually by the colors used in the picture, which correspond to its positions for the relevant years [61].

Chapter 3

Results

3.1 Monthly variation of EEJ

Figure 3.1 illustrates the monthly average of the EEJ for the year 2018. The horizontal axis shows the universal time (UT), which is shared by both observatories, and the vertical axis depicts the EEJ strength, measured in nT (nanotesla). There is a three-hour difference between local time (LT) and UT. Here we note that EEJ remains constant at zero throughout the night and early hours, indicating little activity during these times. The EEJ does, however, typically reach its peak in the late afternoon.

Notably, we regularly noticed negative deflections in the EEJ strength during the local morning and evening hours. The westward current flows during these times, which is a result of the local vertical and zonal winds at E-region altitudes. However, as time goes on, the eastward electric field eventually outperforms the westward current, changing the direction of the EEJ.

The blue curve in Fig. 3.1 shows the EEJ average strength for the month of January. Currents usually move westward at 06 LT (Local Time) in the morning. However, the current's flow changes an hour later, at roughly 07 LT, and eastward currents dominate for the rest of the day. This change suggests that the large-scale background electric field began to move from west to east around 08 LT. The lowest recorded EEJ for January is -4.31 nT at 07 LT. Subsequently, the current strength increases rapidly in the following hours, reaching its peak value of 82.84 nT around 13 LT. The current density steadily drops throughout the afternoon and finally disappears around 18 LT.

In contrast, the minimum value of EEJ occurs in August, having a peak value 23.15 nT at 10.5 LT, while the minimum value of -21.4 nT is observed at 7.5 LT.

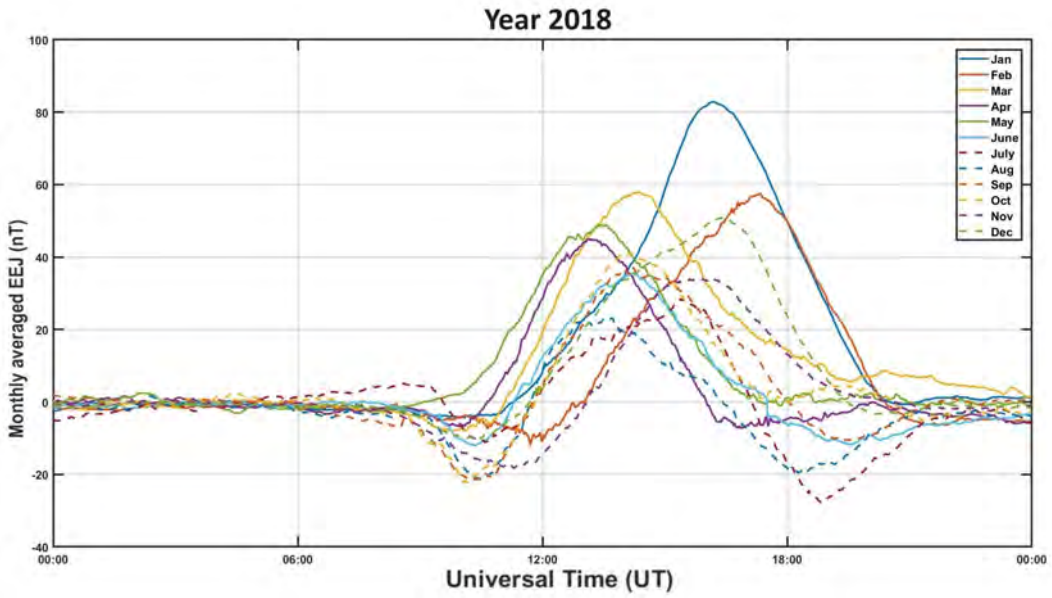

Figure 3.1: Monthly averaged strength of EEJ (nT) versus universal time (UT) for the Year 2018.

The EEJ monthly trend for the year 2019 is depicted in Fig. 3.2, EEJ is here one notice that the absent early in the day and late night, which is caused by a lack of solar activity. The CEJ then appears, and this is reversed by an eastward electric field, resulting in the appearance of EEJ peaks.

The most notable value in 2019 occurred in the month of April when EEJ peaked at 53.98 nT around 11 LT. On the other hand, during the same month, the lowest value of -10 nT CEJ was recorded at 07 LT.

On the other hand, August exhibited the lowest monthly peak, registering a modest 11.2 nT at 13 LT. At 08 LT, the lowest reading for this month was -26 nT. The scene was also dominated by a positive current an hour later, with its maxima appearing about mid-day and gradually fading to zero in the late-night hours.

The monthly distribution of the EEJ for the year 2020 is shown in Fig. 3.3. Due to low solar activity, the EEJ is missing in the early morning and late at night. Every month in 2020 follows the same EEJ trend, i.e. negligible in the morning, gradually falling to a low point at 09 LT, then rising to its highest values before falling back to zero in the late-night hours as presented in Fig. 3.3.

The most noticeable EEJ peak, hitting 55.11 nT approximately 11 LT, in October 2020. On the other hand, at 06 LT in the same month, the lowest reading of -9.6 nT CEJ was noted.

The lowest monthly high of the year (lowest peak value shown by month in the year)

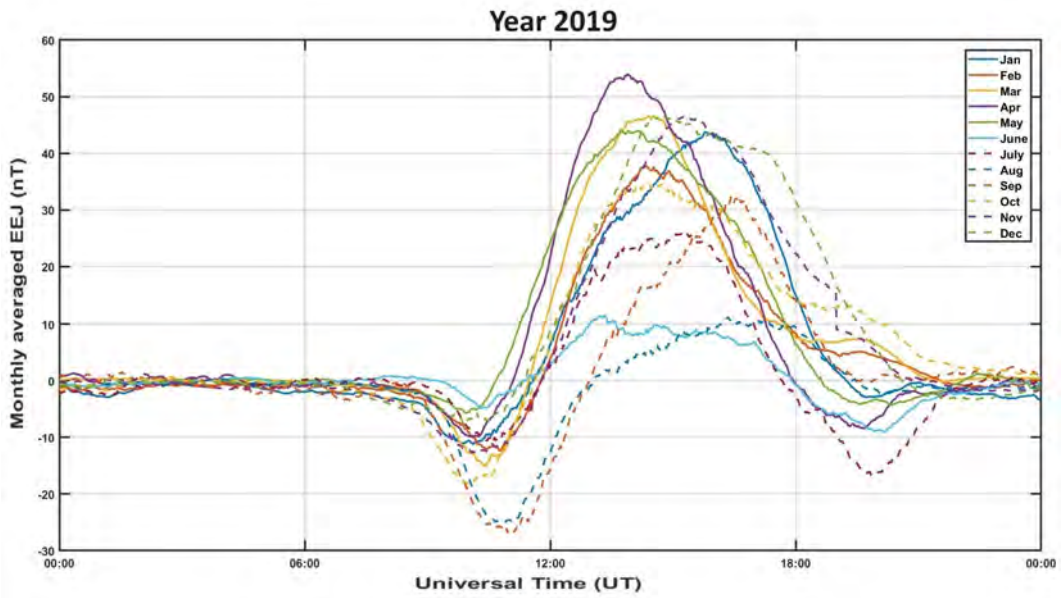

Figure 3.2: The variation in the monthly average strength of the EEJ is plotted against UT for the year 2019.

occurred in June when a modest 7 nT at about 13 LT was recorded. The minimum value for this month was recorded around -17 nT at 08 LT. Then, an hour later, a positive current dominance was noticeable, peaking at noon and gradually fading to zero in the late hours of the night.

The EEJ's monthly distribution for the year 2021 is presented in Fig. 3.4. Surprisingly, as shown in Fig. 3.4, were comparable to the monthly averages for December, January, and March. This graph also fallow the same trend as discuss above and exhibits minimum at 07 LT and then gradually rise to its peak value. The EEJ had its most notable peak in January 2021, soaring to a remarkable 59.70 nT at 11 LT. The EEJ reached its lowest peak during the same month, registering at -9.6 nT at 06 LT, creating an inverted situation.

The lowest monthly high, however, was only a modest 7 nT at 13 LT in June, painting a quite different picture. Additionally, the EEJ decreased to its lowest value of around -17 nT at 08 LT. It's interesting to note that an hour later, a strong positive current took control of the situation. It peaked at noon and steadily declined to zero in the late hours of the night.

Figure 3.5 demonstrated the monthly distribution of the EEJ for the year 2022. Unexpectedly, the EEJ strength this year seems to be distorted, and there is a minor noise in the data. The EEJ reached its most astounding high in September 2022, rising to 83.9 nT at 10.9 LT. Although the EEJ recorded its lowest peak in that same month, most likely due to a westward electric field, measuring -25.5 nT at 15 LT.

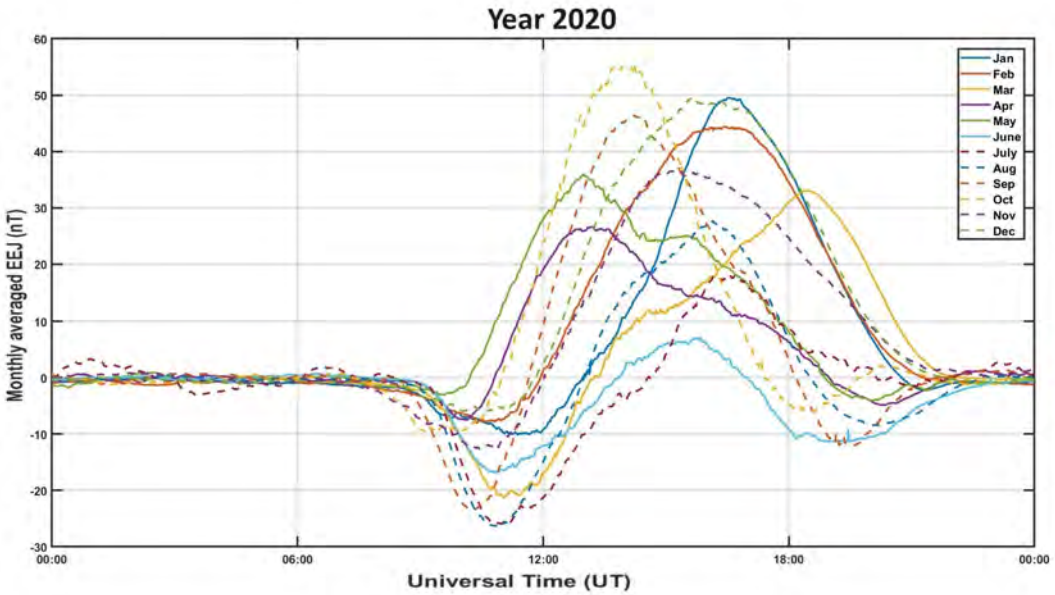

Figure 3.3: Within the timeline of the year 2020, the EEJ's monthly average strength in nT is charted against UT, revealing its dynamic variation.

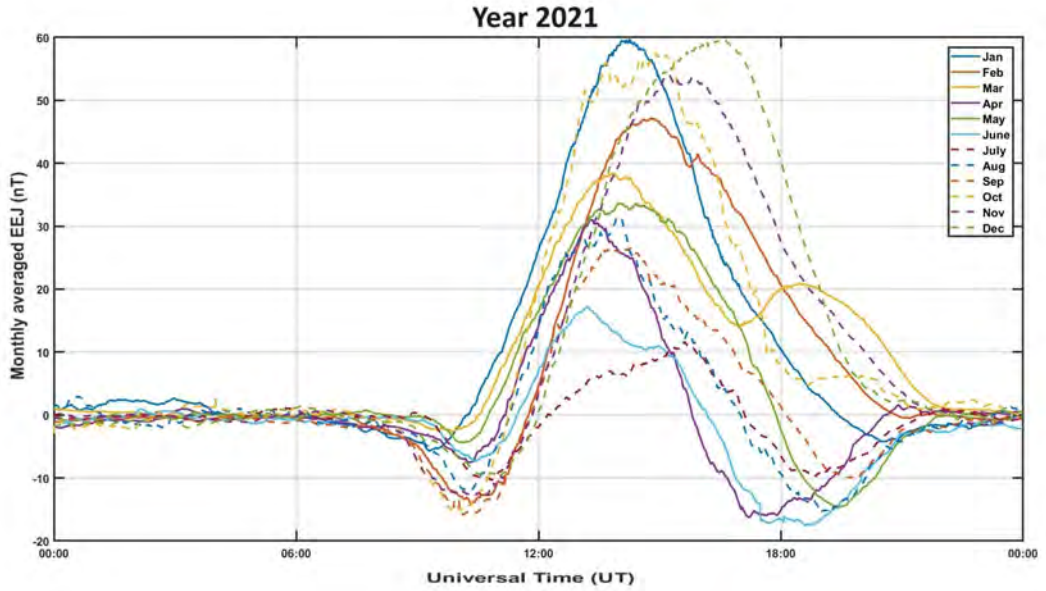

Figure 3.4: During the entirety of 2021, the EEJ's average strength in nT for each month is graphed against UT.

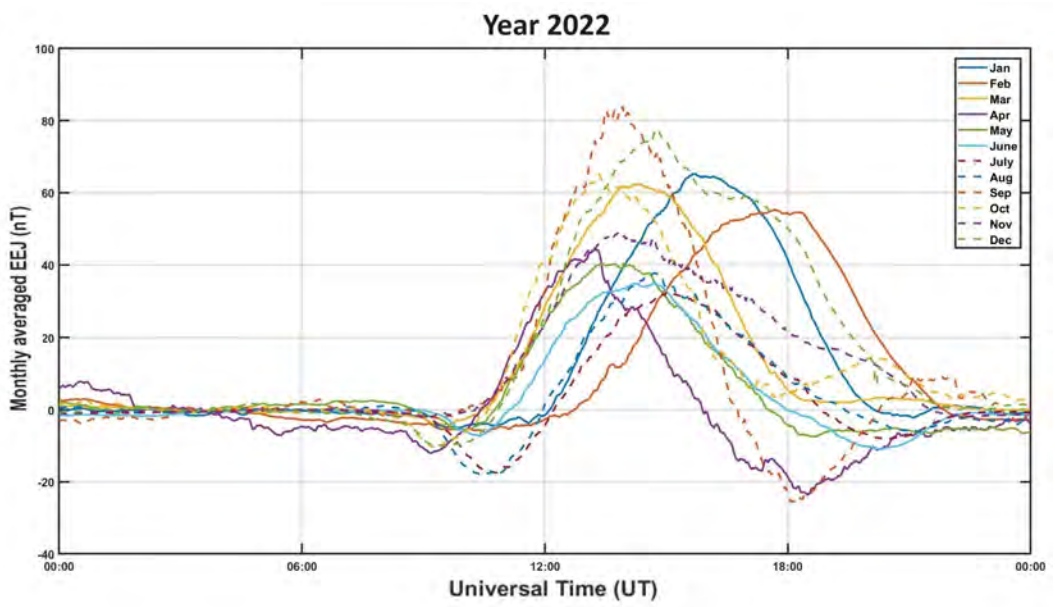

Figure 3.5: Over the course of 2022, the EEJ's monthly average strength in nT is graphically represented against UT, providing a visual demonstration of its fluctuations and changes throughout the year.

July presents a distinct picture, with the lowest monthly high measured at 32.7 nT about 12 LT around -17.4 nT at 08 LT. These results highlight the flexible the EEJ's behavior will be in 2022.

3.2 Annual Variation of EEJ

We're going to analyze the yearly changes in the EEJ. On the x-axis, we'll have the time represented in the universal time frame, while the vertical axis will depict the Average EEJ in nanoteslas. Figure 3.6 illustrates the annual variation for the year 2018. It displays a peak of 34 nT, showcasing a consistent pattern of the EEJ. This pattern starts with a westward EEJ in the early morning, gradually increasing and reaching its peak around noon. Subsequently, the current decreases, approaching zero and sometimes even turning negative during the night.

Figure 3.7 depicts the annual variations in the EEJ for the year 2019. It exhibits a peak at 33 nT, indicating a consistent EEJ pattern. The sequence begins with a westward EEJ in the early morning, progressively intensifies, reaches its zenith around noon, and then gradually diminishes.

In 2020, the EEJ is documented at 27 nT, as depicted in Figure 3.8. During the early hours and late night, the EEJ index registers at zero. Notably, 2020 exhibits the lowest peak in our analysis for this study.

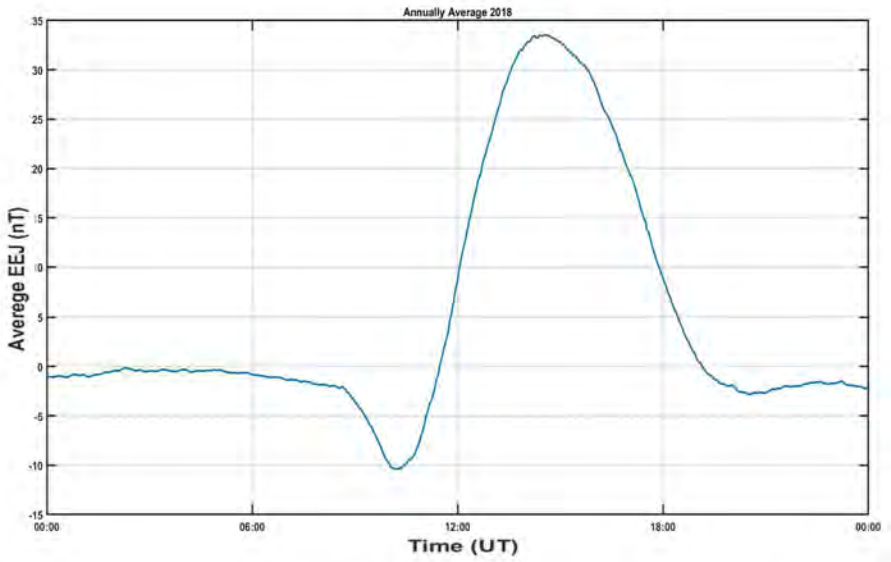

Figure 3.6: Annual variation of EEJ for year 2018.

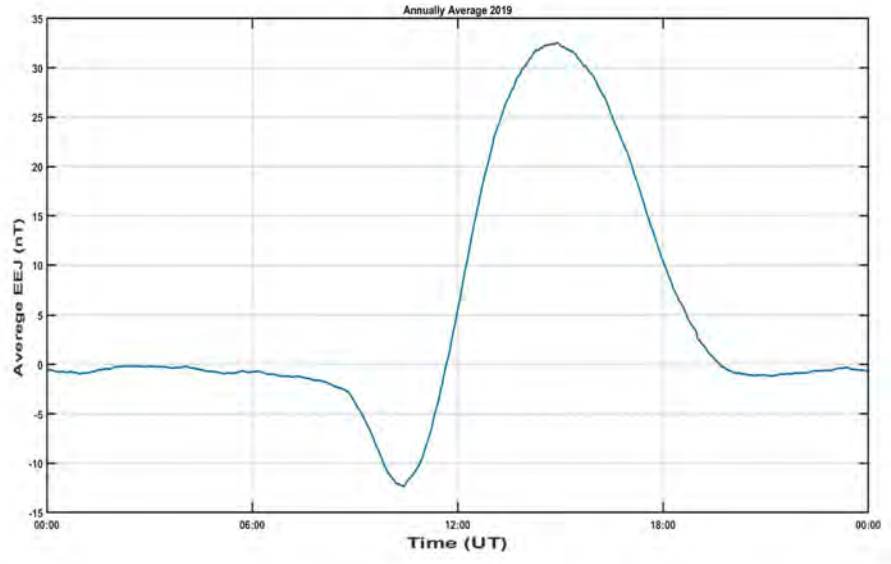

Figure 3.7: The yearly fluctuation of the EEJ in(nT) during 2019.

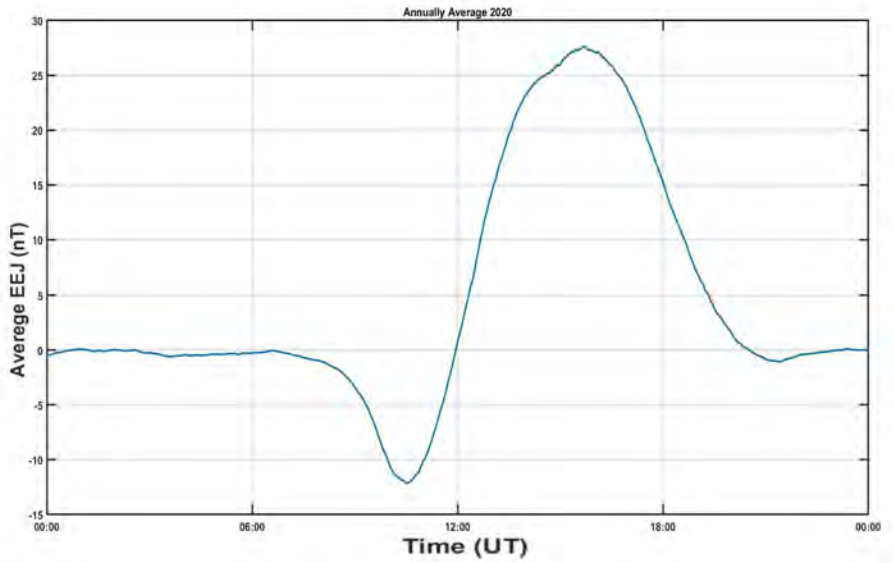

Figure 3.8: The variation in EEJ values throughout the year 2020, measured in nT.

In 2021, the EEJ value reached its peak at 35 nT, as depicted in Fig. 3.9. Moving on to 2022, our analysis reveals an even higher peak value of 46 nT, as illustrated in Fig. 3.10. In summary, 2020 exhibited the lowest EEJ peak value, while 2022 recorded the highest EEJ index in our study.

3.3 Seasonal variation of EEJ from 2018 to 2022

The seasonal variance of the EEJ throughout the year will be discussed in this section. The March equinox, covering the months of February, March, and April; the June solstice, covering the months of May, June, and July; the September equinox, covering the months of August, September, and October; and finally, the December solstice, covering the months of November, December, and January. We will examine the fluctuations of the EEJ varies throughout each of these seasonal years.

Four independent graphs are shown in Fig. 3.11, each of which represents a different season in the year 2018. Figure 3.11 demonstrated that the absence of EEJ in the early morning hours is consistent throughout the entire 2018, showing that there is no solar activity at that time. The CEJ begins to gradually appear at 06 LT, and an hour later it reaches its peak strength. After then, an eastward current takes over, reaching its heights about mid-day and gradually fading until late at night. This pattern is evident in all four seasons and offers useful data on the EEJ's behavior throughout the year 2018 at various times of the day.

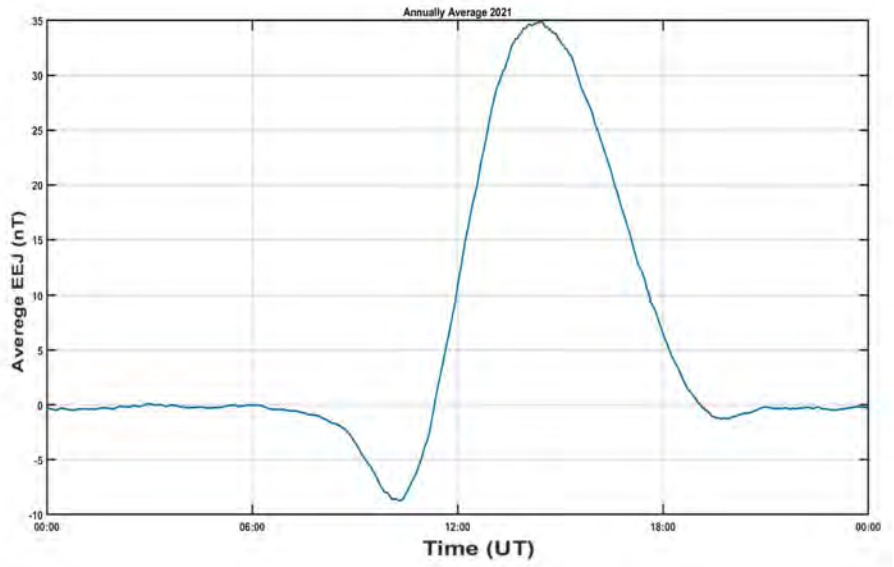

Figure 3.9: The annual EEJ fluctuations for the year 2021, represented in nT.

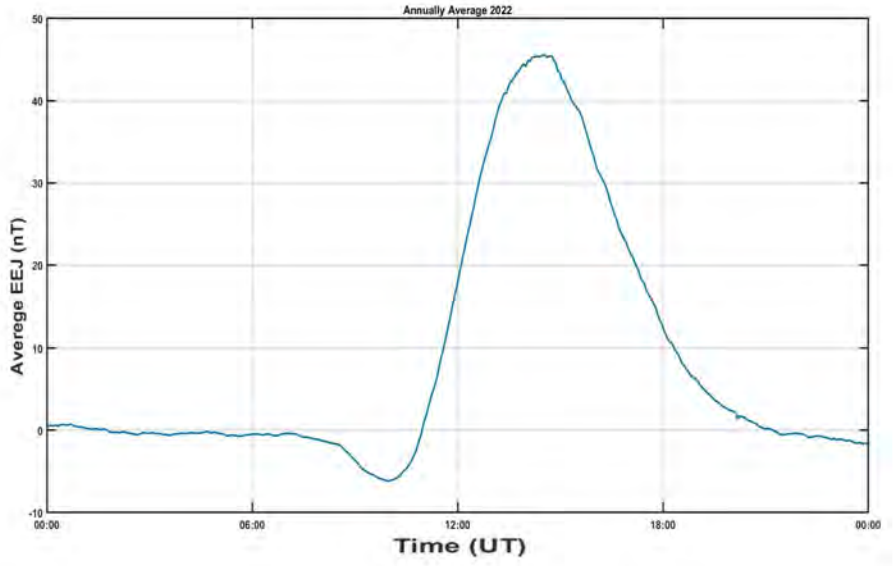

Figure 3.10: Annual variation of EEJ for year 2022.

It is clear from Fig. 3.11 that the EEJ reaches a remarkable peak value at the December solstice, reaching the value of 55.62 nT at an average time of 13 LT. The lowest reading of -10.5 nT, on the other hand, is noted at 07:30 LT. The December solstice graph displays a smooth curve throughout the year, initially showing no current, but with time, a westward current appears. After that, an eastern electric field takes over, gradually causing a peak to appear about mid-day. The stream gradually drops off until it vanishes as one approaches night-times. This observed pattern sheds light on the distinct behavior of the EEJ during the December solstice, offering valuable insights into its dynamics and variation during this specific period.

The March equinox reaches its second peak, as depicted in Fig. 3.11, with the highest reading for this season being 38.15 nT recorded at 11:15 LT. The EEJ intensity exhibits a similar pattern at the March equinox as it does during the December counterpart. At 06:43 LT, the lowest value is recorded during this time namely -6.14 nT. The June solstice, on the other hand, has a high value of 33.09 nT at 10:50 LT and a minimum of -12.62 nT at 15:52 LT.

The September equinox in the studied year has the lowest peak value, which was recorded at 32.4 nT at 11:14 LT. It's interesting to note that this season also exhibits the lowest minimum value for the EEJ at -21.21 nT at 07:16 LT. As a result, Fig. 3.11 presents that the September equinox has the lowest value while the December solstice has the highest value. Significant insights into the EEJ's behavior over the numerous seasonal transitions throughout the year may be gained from these unique peaks and lowest levels. These data demonstrate diverse patterns and behaviors during each particular season of the year, as well as the varied peak values and oscillations of the EEJ across time.

According to Fig. 3.12, the EEJ surges to 45.34 nT at an average time of 11:14 LT during the March equinox for the year 2019. In contrast, the EEJ's lowest recorded value was -11.74 nT at 07:14 LT. Figure 3.12 depicted a second peak at the December solstice, with the highest value for this season being 44.52 nT at 12:22 LT. The EEJ's intensity pattern at the March equinox closely follows that of the December solstice. Its lowest value, measuring -10.1 nT at 07 LT, was recorded. On the other hand, the June solstice shows a maximum value of 25.52 nT at 10:44 LT and the lowest value of -6.4 nT at 07:17 LT.

The September equinox displays the year's lowest peak value, which was measured at 23.56 nT around 13:21 LT. The lowest minimum value for the EEJ, at -21.24 nT at 07:35 LT, is also interestingly displayed during this season. Thus, the September equinox stands out in Fig. 3.12 as having the lowest values, while the March equinox stands

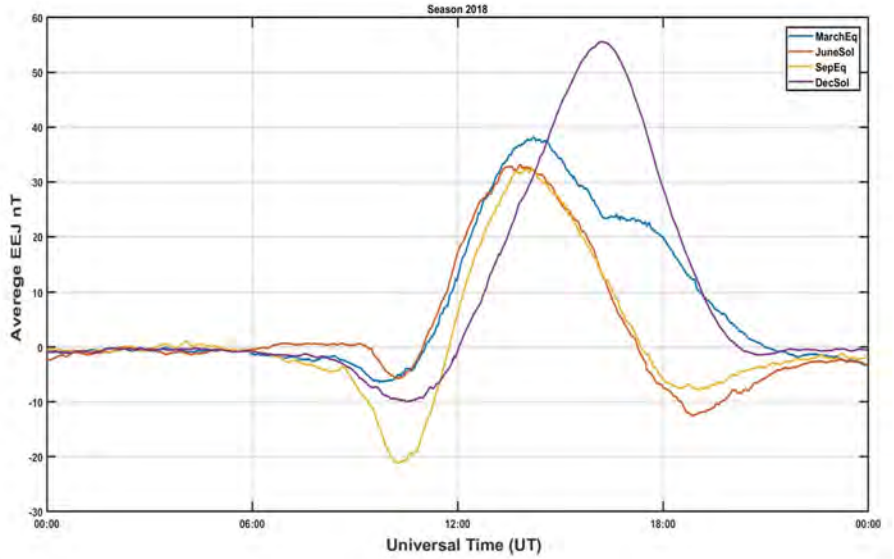

Figure 3.11: Seasonal variation of EEJ verus UT for year 2018.

out as having the highest values. Notably, the comparison of the years 2018 and 2019 reveals a recurring pattern in which the September equinox consistently coincides with the lowest peak values and the lowest minimum values.

Figure 3.13 illustrates significant changes in the EEJ for the year 2020. The December solstice has the maximum intensity, with a value of 44.07 nT at an average time of 13:23 LT. On the other hand, at 07:51 LT, the EEJ reached its lowest recorded value of -9.06 nT. Figure 3.13 depicts a significant peak at the September equinox, reaching 39.35 nT at 11:20 LT. The lowest value, however, measuring -18.29 nT, is noted at 07:22 LT. On the other hand, the March equinox shows a peak value of 26.36 nT at 13:57 LT and the lowest value of -9.92 nT at 07:36 LT.

The June solstice, on the other hand, exhibits the lowest peak value for the whole year, measuring 14.95 nT around 13 LT. Additionally, at 07:31 LT, -11.95 nT is noted as the EEJ's lowest reading for the whole year. These distinctive observations demonstrate the various EEJ intensity levels during several seasons in the year 2020. For instance, the June solstice has the lowest peak value, while the December counterpart stands out with the largest peak.

In Figure 3.14, the year 2021 unveils distinctive patterns in the EEJ across its seasonal transitions. Notably, the EEJ value for the December solstice is highest at 53.34 nT at 12:05 LT and the lowest at -7.39 nT at 06:45 LT. The September equinox, on the other hand, achieves its maximum strength of 36.97 nT at 10:56 LT and its minimum level of -14.14 nT at 07:08 LT. The March equinox has a peak EEJ intensity of 36.13 nT at

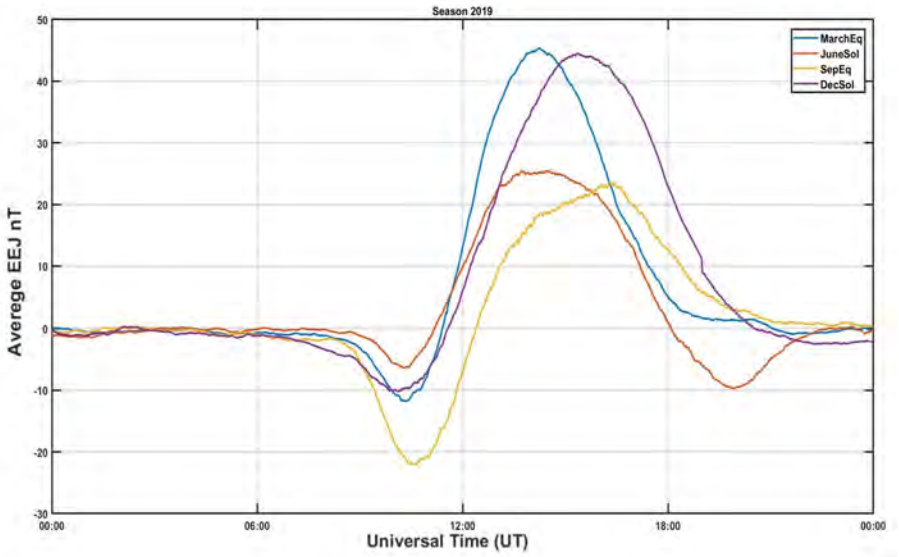

Figure 3.12: During the entirety of 2019, the EEJ's seasonal variation was charted with respect to UT.

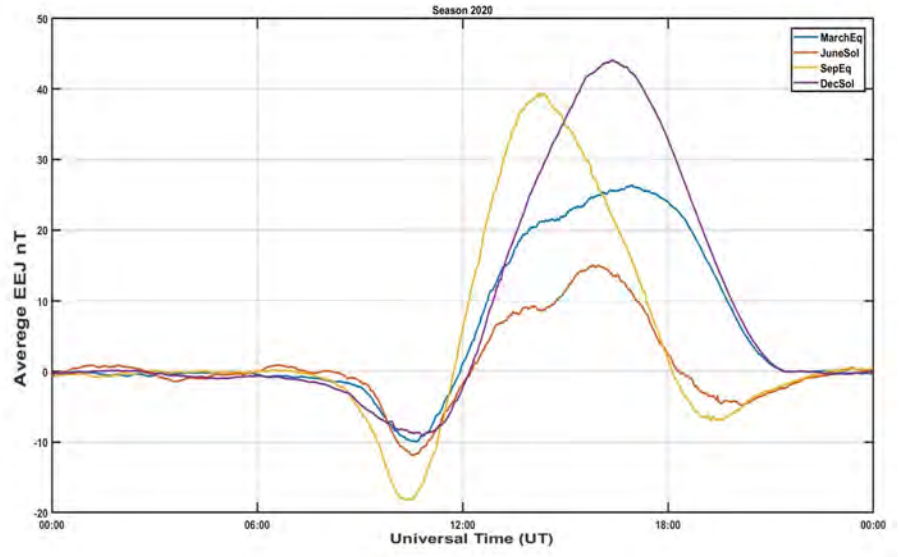

Figure 3.13: Throughout the year 2020, the EEJ was graphed against UT to observe its seasonal fluctuations.

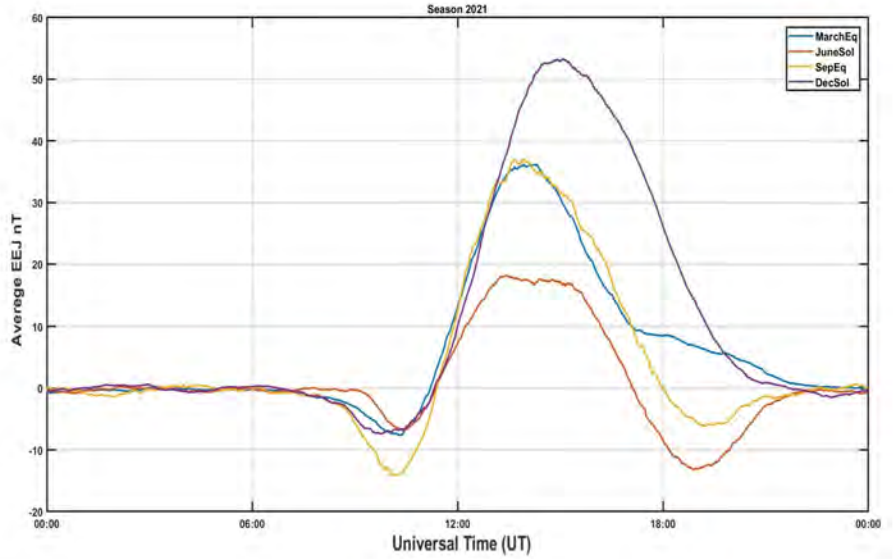

Figure 3.14: The EEJ strength's seasonal variation vs UT for the year of 2021.

11:17 LT, while its lowest value registers -7.65 nT at 07:19 LT. It's interesting that the June solstice records the lowest peak for the whole year, measuring 18.18 nT at 10:25 LT, while its lowest EEJ strength hits -13.1 nT at 15:59 LT. These thorough studies provide an insight into the EEJ's intensity variations during each season in 2020.

When examining Fig. 3.15, we can see that the EEJ had a significant increase to 59.02 nT at the December solstice for the year 2022, which was recorded at an average time of 11:43 LT. At 06:35 LT, on the other hand, the EEJ decreases to its lowest recorded value of -5.3 nT. It is noteworthy that the EEJ reaches its maximum value for this season at the second peak visible during the March equinox, hitting 58.3 nT at 10:55 LT. Interestingly, the intensity pattern of the EEJ at the September equinox closely resembles that of the December solstice, with a significantly low value of -7.38 nT measured at 07:00 LT. The March equinox, on the other hand, has a peak value of 36.64 nT at 11:27 LT and a minimum value of -6.84 nT at 06:19 LT.

The EEJ has its lowest peak value of the year on the June solstice, measuring 33.85 nT at around 11:35 LT. Additionally, during this season, the EEJ's lowest minimum value of -9.12 nT was observed at 07:25 LT. Therefore, Fig. 3.15 vividly illustrates the various seasonal fluctuations in EEJ intensity, with the December solstice standing out for its notable rise and the June solstice being recognized for its lowest levels.

In table 3.1 we have summarize all the results as discussed above. i.e. maximum daytime values for EEJ (nT) for the various seasons of the year 2018-2022.

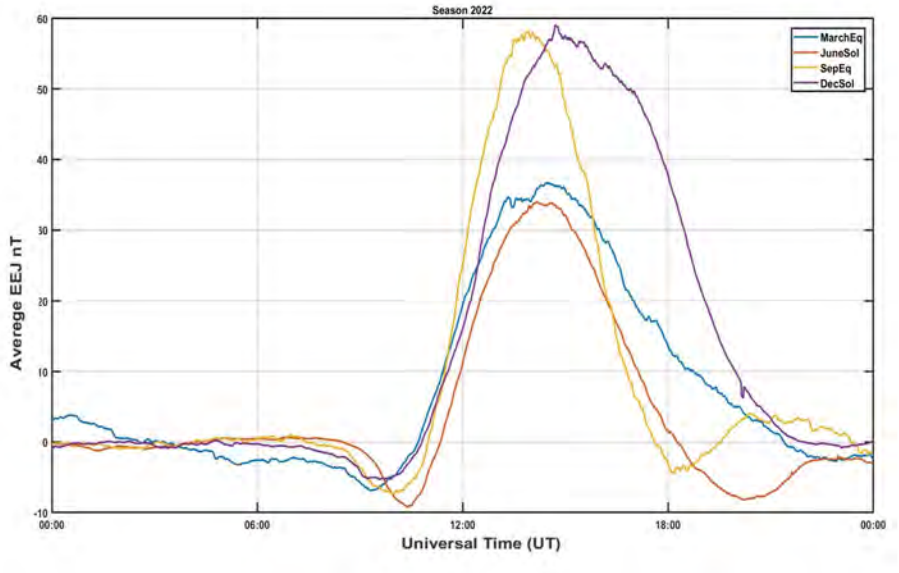

Figure 3.15: The year 2022 witnessed the seasonal variation of the EEJ strength plotted against UT.

Maximum day-time EEJ (nT)					
Year	2018	2019	2020	2021	2022
March Equinox	38.15	45.34	26.36	36.13	36.64
June solstice	33.09	25.52	14.95	18.18	33.85
September Equinox	32.4	23.56	39.35	36.97	58.3
December solstice	55.62	44.52	44.07	53.34	59.02

Table 3.1: The peak EEJ strength was recorded during various seasons over a span of five years.

3.4 Local time of peak EEJ

In Fig.3.16, a bar graph, the horizontal axis denoting the months and the vertical axis denoting LT, depicts the highest values of the EEJ strength for each month. We presents a five-year bar graph from 2018 to 2022 to give a complete picture. As a result, we are able to examine the monthly EEJ peaks and their associated LT. The monthly peak is shown by each bar on the graph, and the height of each bar corresponds to the LT at which the peak occurs.

Here, we look at the patterns of EEJ peaks over the months of particular years to see whether they typically occurs in the late night or early morning. Additionally, we want to know the time of day when EEJ peaks the most frequently on average. By demonstrating the relationship between the monthly peaks and the associated LT, this visualization enables us to learn important details about the temporal variations of the EEJ strength.

Figure 3.16 exhibits five distinct graphs, with each one representing a specific year. The graph for the year 2018 illustrates the EEJ monthly peaks. The bar for April shows the lowest value, suggesting that the peak occurs earlier in the month. The highest peak is seen in February, which indicates that it happens in the evening. Analysis of the data reveals that the peak of EEJ for the year 2018 occurs on average between $10:45$ to $11:45$ LT. With the use of this understanding, we are able to track the EEJ peaks' diurnal patterns over the course of the year's several months.

The statistics presented in Fig. 3.16 show that there are clear trends in EEJ strength for the year 2020. The month of May has the lowest bar length, indicating an earlier occurrence than other months in 2020, but March stands out for having an apparent peak. Furthermore, between $12:30$ and $13:30$ this year, the average time period with the largest concentration of EEJ peaks were found. The fact that over half of the peaks appear during this time frame indicates a major temporal trend for the year 2020, with March standing out as a month with a high peak, these findings offer light on the temporal fluctuations in the EEJ strength throughout various months of 2020. The month of May, however, emphasizes early occurrences.

For the years 2021 and 2022, various trends regarding the EEJ strength may be shown in Fig. 3.16. December, denotes a notable peak, while the shortest bar, in June, denotes its early occurrence than other months in 2021. Additionally, the peak of EEJ strength for the year 2022 arrives earlier in October, although February has the longest bars, indicating a significant surge during this month. The average time period of the day for

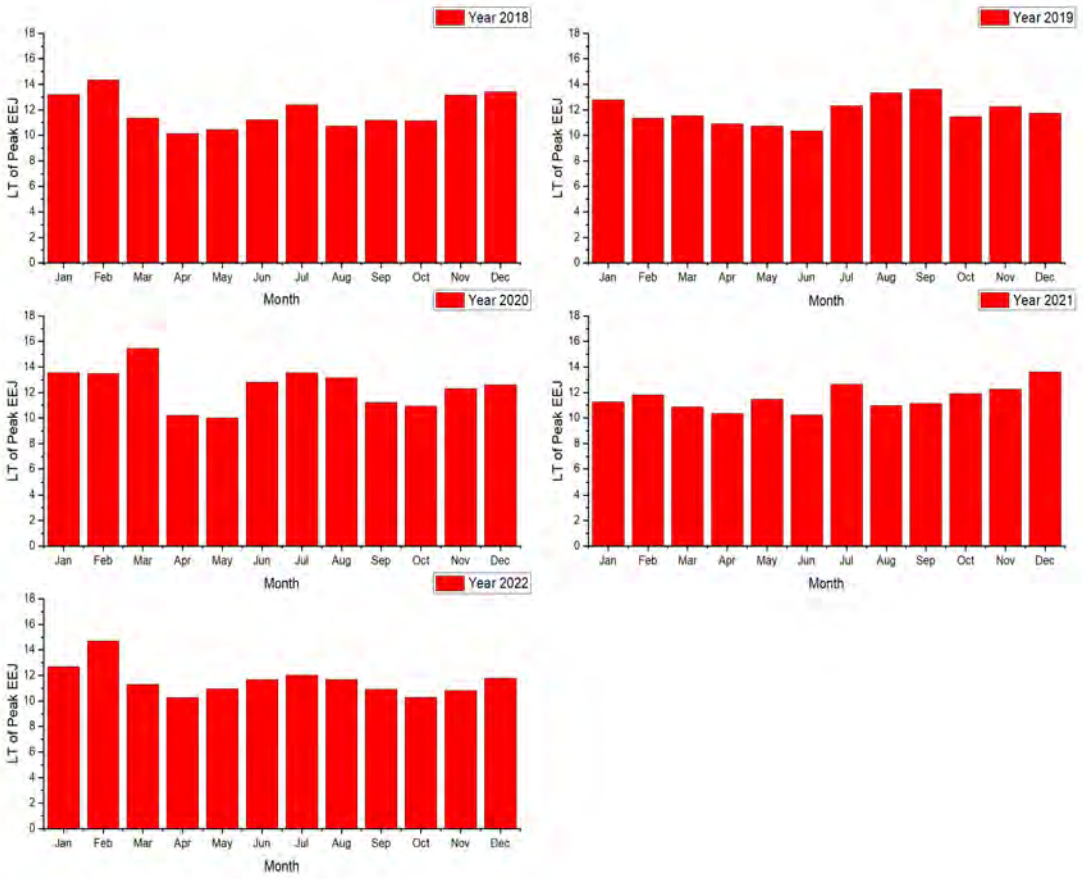

Figure 3.16: The LT peak for EEJ for the period 2018-2022.

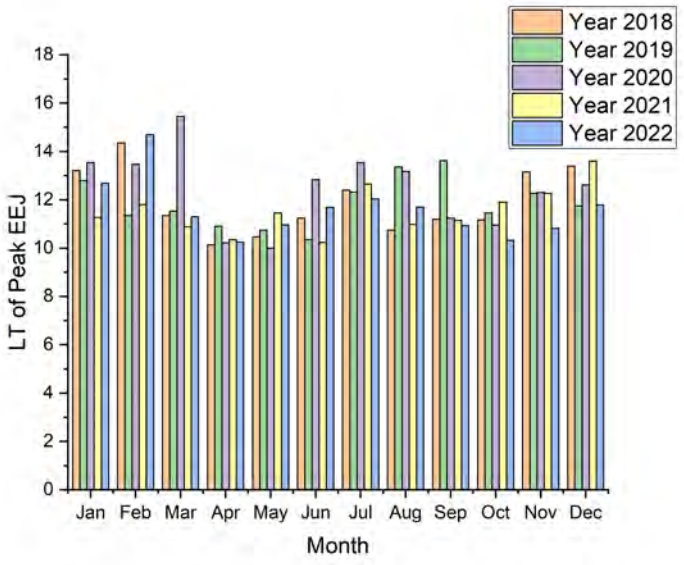

Figure 3.17: Comparative analysis of EEJ Peaks versus LT from 2018 to 2022.

this year, during which the greatest number of EEJ peaks take place, is between $10:20$ and $11:20$ LT.

Figure 3.16 highlights us an extensive overview of the LT peaks of the EEJ from 2018 to 2022, enabling us to determine the timing of peak occurrence. By comparing the five graphs, we note that for the year 2020, the peak of EEJ in May appears before it does in any other month and that the bar length in March is the longest of all the years that have been observed. These data help us to understand the unique behavior of the EEJ from 2018 to 2022 by providing important insights into the temporal fluctuations of the EEJ intensity across various months and years.

The EEJ for five consecutive years is compared and plotted against LT hours in Fig. 3.17. Particularly, the focus is to analyzing the EEJ behavior for the same month throughout the span of five years. We want to pinpoint the year in which the EEJ peak occurs early or late in the day by visualizing the data. For instance, the first five bars in Fig. 3.17, which show the EEJ peaks versus the corresponding LT hours, represent the months of January from 2018 to 2022, respectively. Upon examination, we see that the peak for January in the year 2021 happens earlier in the day than it does in 2020. By comparing the five years under examination, we can identify the periodical fluctuations of the EEJ peak in January. Furthermore, we can examine the behavior of every month from 2018 through 2022 due to further investigation in Fig. 3.17. We can determine whether the EEJ demonstrates maximal intensity in the morning or at noon by examining the peaks of each month.

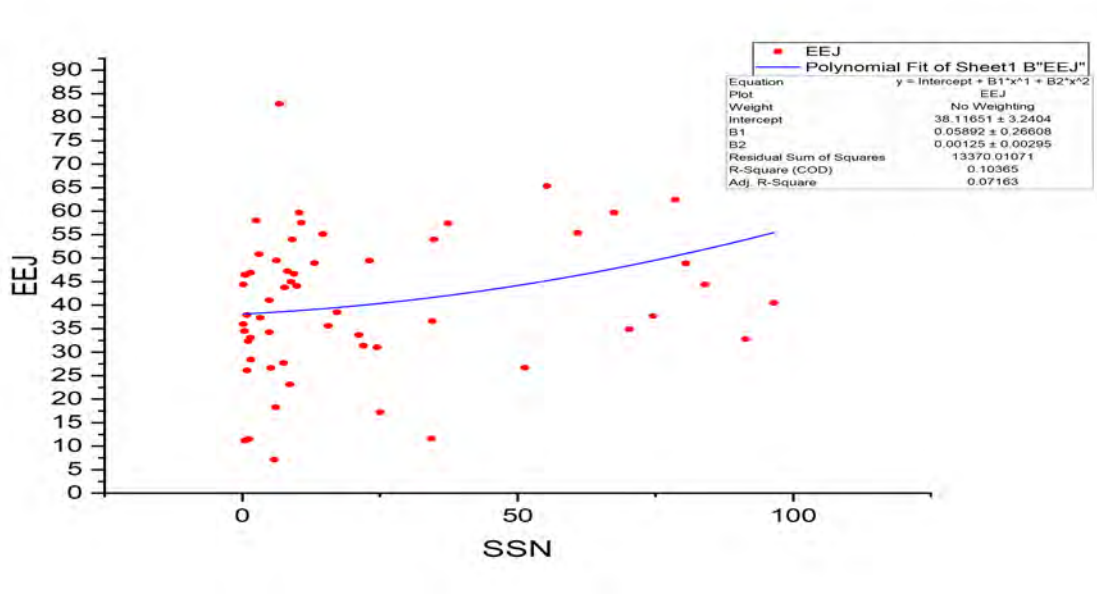

Figure 3.18: Comparison of EEJ Peaks and SSN.

3.5 Correlating EEJ peaks with SSN

We provide a scatter graph in Fig. 3.18 showing the relationship between the EEJ peak and SSN. Here the EEJ peak values are displayed on the vertical axis and SSN values are plotted on the horizontal axis for the data, which covers the period from January 2018 to November 2022. After examining the scatter plot and using a polynomial fitting method, we find that a substantial portion of EEJ peaks lie between 0 and 15 SSN values. Notably, the SSN range of 0 to 50 includes over 80% of the EEJ peaks,

this phenomenon can be attributed to the fact that a significant portion of the data set is concentrated within the solar minimum cycle. It is clear from Fig. 3.18 that increasing SSN are correlated with increasing EEJ intensity. However, polynomial fitting, as shown in Fig. 3.18, reveals a discernable pattern, highlighting the obvious connection between increasing SSN and intensifying EEJ.

Chapter 4

Discussion of results

In our analysis of EEJ, five-year monthly averaged data, the following trends can be seen. On average, December has the highest value in almost all the cases of interest, while January depicts the second largest EEJ index. On the other hand, across these years, June and July frequently exhibit the lowest and second-lowest EEJ values, respectively. Based on these findings, we can anticipate that December and January typically provide the highest EEJ values, however, June and July yield the lowest values, reversing the pattern. Also, the study investigated the seasonal variation of the EEJ over five years. In most years, the EEJ's peak strength occurred during the December solstice, but in 2019, it was similar to the March equinox. On average, the EEJ's lowest strength was consistently observed during the June solstice, with the March and September equinoxes showing intermediate values between those observed during the December and June solstices. This trend can be to associated to the phenomenon known as annual asymmetry (Winter Anomaly), which states that the yearly ionospheric asymmetry constitutes a 20–40% increase in the global F layer plasma density in December/January compared to that in June/July [62]. Azpilicueta and Brunini (2011) suggested that energy transfer from the magnetosphere to the ionosphere might be another mechanism for the annual asymmetry [63] [64]. The EEJ intensity appears to be lower at the June solstice than the December counterpart. When compared to the December solstice, the June solstice signifies the start of the local summer, which suggests a higher ionospheric conductivity. However, this alone should not explain the observed difference in EEJ intensity between these two seasons. Instead, local wind patterns are probably responsible for the observed discrepancy. Yacob (1975) and other earlier investigations have noted that the dip-equatorial amplification of Sq fields is at its lowest during the local summer in the Indian sector [65]. According to Hutton (1967),

similar patterns may be seen in the EEJ profiles in the south American territory. This apparent winter-summer asymmetry in EEJ intensity does not appear to be specific to the East Asian area but rather to be a generic phenomenon. Using satellite data, Le Moul et al. (2006) demonstrated that the summer is when EEJ intensity is at its lowest [65].

Plotting the LT peak of the EEJ over five years allowed us to investigate how it changed throughout the day and to know that when does a peak occurs. According to the data, most of the monthly EEJ peaks consistently were observed between 11 and 13 LT around noon. A considerable concentration of intensive activity was present during those hours, as evidenced by the fact that most of the highest values of EEJ ever recorded occurred within the specified period [66]. Because of the significant influence of the ionization process, which is common around noon, on the Earth's ionosphere, the current strength is consistently higher during these hours [67]. In an earlier work, Rastogi and Iyer (1976) noticed that during the period from 1958 to 1959, the daily fluctuation of the horizontal component of the Earth's magnetic field near magnetic equatorial stations peaked after noon LT [68]. Doumouya et al. (2003) developed an empirical model for the EEJ that uses magnetic information from 26 observatories dispersed over six longitudinal sectors. They suggested that the local time and longitude had a major impact on how the EEJ behaved. They used the general theory that the EEJ peak value often occurred at approximately noon LT. However, they considered that slight deviations of up to ±1 hour were also possible [68].

The zonal (east-west) electric field as well as the local electrical conductivity both have a significant impact on the EEJ's strength. Due to the effects of solar radiation, the conductivity peaked at noon. On the other hand, neutral winds produced by the forces of gravity of the Sun and Moon, as well as the ionosphere's heating from solar radiation, produced the zonal electric field. This implied that the zonal electric field's peak intensity might occur at precisely noon. Due to these complex interactions, a significant concentration of EEJ peaks was frequently seen around noontime [68].

We have also presented the peak values of the EEJ against their corresponding SSN index, and employed a polynomial fitting approach to show the correlation between the intensity of the EEJ and the SSN. It is observed that an increasing SSN is correlated with an increasing EEJ strength. During the maximum solar cycle between 2011 and 2013, there was a general upswing in the strength of the EEJ across all regions [69]. Increased solar activity levels have led to increased ionospheric heating, which is the cause of this occurrence. This increased solar activity also results in a larger intake of

energetic particles, which helps to produce stronger electric fields and winds [70]. As a result, this interaction causes the EEJ's total intensity to significantly increase.

Chapter 5

Summary

In this dissertation, we have examined the Equatorial Electrojet (EEJ) and some of its distinctive features, including its seasonal and twilight changes and its relationship to the Solar Sunspot Number (SSN). Our study is methodically structured, starting with fundamental concepts and a thorough analysis of the problem at hand, following the historic research in this field. This initial exploration helps to establish a solid grasp of the fundamental concepts within the domain of our research area.

We then explain the characteristics of our dataset and the methods used throughout this study. The dataset, which we obtained from ground-based magnetic observatories, spans a continuous five-year period from 2018 to 2022. These observatories are connected to the website resource "INTERMAGNET." For the analysis of EEJ an off-separation method has been employed that provides a measure the strength of the EEJ index. In this method, data from off-equator observatories are separated from those from equatorial observatories. We determine the effect of EEJ on the ionosphere by examining the changes in the magnetic field.

As the ionosphere has a significant impact on the transmission of radio waves, with its effectiveness influenced by the density of the EEJ. Therefore, changes in the EEJ hold great importance for the everyday communications. We analyze the fluctuations in EEJ across different seasons and times of day, as well as the effect of SSN on the variations of EEJ.

To conclude, here is the short description of our results.

1- According to our analyses, most of the monthly EEJ peaks were observed between 11 and 13 LT around the noon time. A considerable concentration of intense solar activity was present during those hours, as evidenced by the fact that most of the highest values

ever recorded occurred within the specified period.

2- The EEJ intensity appears to be lower at the June solstice than it's December counterpart. This trend can be associated with the phenomenon known as annual asymmetry, according to which the yearly ionospheric asymmetry constitutes increase in the global F layer plasma density in December/January compared to that in June/July.

3- We have also represented the peak values of the EEJ against their corresponding SSN and employed a polynomial fitting approach to analyze the trends. The illustration shows a direct relationship between the intensity of the EEJ and the SSN, namely an increasing SSN corresponds well to an increasing EEJ strength.

Bibliography

[1] FO Grodji, V Doumbia, K Boka, Christine Amory-Mazaudier, Y Cohen, and Rolland Fleury. Estimating some parameters of the equatorial ionosphere electrodynamics from ionosonde data in west africa. *Advances in Space Research*, 59(1):311–325, 2017.

[2] Hermann Lühr, Patrick Alken, and Yun-Liang Zhou. The equatorial electrojet. *Ionosphere Dynamics and Applications*:281–299, 2021.

[3] Denis Grodent, JT Clarke, J Kim, JH Waite, and SWH Cowley. Journal of geophysical research. space physics, 2003.

[4] Information for Kourou (KOU) Geomagnetic Observatory — wdc.bgs.ac.uk. `http://www.wdc.bgs.ac.uk/obsinfo/kou.html`. [Accessed 06-Jul-2023].

[5] Information for Tatuoca (TTB) Geomagnetic Observatory — wdc.bgs.ac.uk. `http://www.wdc.bgs.ac.uk/obsinfo/ttb.html`. [Accessed 06-Jul-2023].

[6] John Ashworth Ratcliffe et al. *An introduction to ionosphere and magnetosphere*. CUP Archive, 1972.

[7] N Balan, GJ Bailey, B Jenkins, PB Rao, and RJ Moffett. Variations of ionospheric ionization and related solar fluxes during an intense solar cycle. *Journal of Geophysical Research: Space Physics*, 99(A2):2243–2253, 1994.

[8] Bhattacharyya Archana, Kakad Bharati, Gurram Padma, Sripathi Samireddypalle, and Sunda Surendra. Effect of magnetic storms on the development of scintillation-producing irregularities in low latitude ionosphere. In *VarSITI-Variability of the Sun and Its Terrestrial Impact*, pages 74–74, 2017.

[9] Lihui Qiu, Tao Yu, Xiangxiang Yan, Yang-Yi Sun, Xiaomin Zuo, Na Yang, Jin Wang, and Yifan Qi. Altitudinal and latitudinal variations in ionospheric sporadic-e layer obtained from formosat-3/cosmic radio occultation. *Journal of Geophysical Research: Space Physics*, 126(9):e2021JA029454, 2021.

[10] Zhou Yiyan, Wu Yun, Qiao Xuejun, and Zhang Xunxie. Ionospheric anomalies detected by ground-based gps before the mw7. 9 wenchuan earthquake of may 12, 2008, china. *Journal of atmospheric and solar-terrestrial physics*, 71(8-9):959–966, 2009.

[11] Kenneth Davies and Donald M Baker. On frequency variations of ionospherically propagated hf radio signals. *Radio Science*, 1(5):545–556, 1966.

[12] Jane L Fox and Arvydas J Kliore. Ionosphere: solar cycle variations. *Venus II*, 349:161, 1997.

[13] Marsha R Torr and DG Torr. The seasonal behaviour of the f2-layer of the ionosphere. *Journal of Atmospheric and Terrestrial Physics*, 35(12):2237–2251, 1973.

[14] T Yonezawa. Theory of formation of the ionosphere. *Space Science Reviews*, 5(1):3–56, 1966.

[15] AP Mitra. The d-layer of the ionosphere. *Journal of Geophysical Research*, 56(3):373–402, 1951.

[16] H Rishbeth. The ionospheric e-layer and f-layer dynamosâa tutorial review. *Journal of Atmospheric and Solar-Terrestrial Physics*, 59(15):1873–1880, 1997.

[17] VV Kuverova, SO Adamson, AA Berlin, VL Bychkov, AV Dmitriev, YA Dyakov, LV Eppelbaum, GV Golubkov, AA Lushnikov, MI Manzhelii, et al. Chemical physics of d and e layers of the ionosphere. *Advances in Space Research*, 64(10):1876–1886, 2019.

[18] Christos Haldoupis. Midlatitude sporadic e. a typical paradigm of atmosphere-ionosphere coupling. *Space science reviews*, 168:441–461, 2012.

[19] R Behnke. F layer height bands in the nocturnal ionosphere over arecibo. *Journal of Geophysical Research: Space Physics*, 84(A3):974–978, 1979.

[20] LiBo Liu, WeiXing Wan, YiDing Chen, and HuiJun Le. Solar activity effects of the ionosphere: a brief review. *Chinese Science Bulletin*, 56:1202–1211, 2011.

[21] J Laštovička. Effects of geomagnetic storms in the lower ionosphere, middle atmosphere and troposphere. *Journal of Atmospheric and Terrestrial Physics*, 58(7):831–843, 1996.

[22] AD Danilov and J Lastovicka. Effects of geomagnetic storms on the ionosphere and atmosphere. *International Journal of geomagnetism and aeronomy*, 2(3):209–224, 2001.

[23] James A Marusek. *Solar storm threat analysis*. J. Marusek, 2007.

[24] JH Dellinger. The role of the ionosphere in radio wave propagation. *Electrical Engineering*, 58(11):803–822, 1939.

[25] Saradi Bora. Ionosphere and radio communication. *Resonance*, 22(2):123–133, 2017.

[26] Yu P Galuk, AP Nickolaenko, and M Hayakawa. Amplitude variations of elf radio waves in the earth–ionosphere cavity with the day–night non-uniformity. *Journal of Atmospheric and Solar-Terrestrial Physics*, 169:23–36, 2018.

[27] RR Belgibaev, NV Ryabova, and EV Katkov. Effects of absorption during solar flares of class m4. 0, m7. 3 and x2. 0 on parameters of cognitive hf communication systems. In *2019 Russian Open Conference on Radio Wave Propagation (RWP)*, volume 1, pages 349–352. IEEE, 2019.

[28] Carine Briand, Mark Clilverd, Srivani Inturi, and Baptiste Cecconi. Role of hard x-ray emission in ionospheric d-layer disturbances during solar flares. *Earth, Planets and Space*, 74(1):41, 2022.

[29] Norbert Jakowski, Christoph Mayer, Volker Wilken, and Mohammed M Hoque. Ionospheric impact on gnss signals. *Física de la Tierra*, 20:11, 2008.

[30] William F Utlaut and Robert Cohen. Modifying the ionosphere with intense radio waves: powerful ground-based radio transmissions are now being used to induce observable ionospheric changes. *Science*, 174(4006):245–254, 1971.

[31] Ahmet Yucel Urusan. Earthquake prediction, ionospheric total electron content, and three earthquakes in california. *Thermal Science*, 2019.

[32] RA Heelis. Electrodynamics in the low and middle latitude ionosphere: a tutorial. *Journal of Atmospheric and Solar-Terrestrial Physics*, 66(10):825–838, 2004.

[33] Mala S Bagiya, KN Iyer, HP Joshi, Smitha V Thampi, Takuya Tsugawa, Sudha Ravindran, R Sridharan, and BM Pathan. Low-latitude ionospheric-thermospheric response to storm time electrodynamical coupling between high and low latitudes. *Journal of Geophysical Research: Space Physics*, 116(A1), 2011.

[34] RA Heelis. Studies of ionospheric plasma and electrodynamics and their application to ionosphere-magnetosphere coupling. *Reviews of Geophysics*, 26(2):317–328, 1988.

[35] AD Richmond. Modeling the ionosphere wind dynamo: a review. *pure and applied geophysics*, 131:413–435, 1989.

[36] R Pratap and Vinod H Gandhi. Tensor conductivity in the ionosphere, 1976.

[37] M Blanc and AD Richmond. The ionospheric disturbance dynamo. *Journal of Geophysical Research: Space Physics*, 85(A4):1669–1686, 1980.

[38] Astrid Maute and Arthur D Richmond. F-region dynamo simulations at low and mid-latitude. *Space Science Reviews*, 206(1-4):471–493, 2017.

[39] AV Streltsov and W Lotko. Multiscale electrodynamics of the ionosphere-magnetosphere system. *Journal of Geophysical Research: Space Physics*, 109(A9), 2004.

[40] RG Rastogi and VL Patel. Effect of interplanetary magnetic field on ionosphere over the magnetic equator. In *Proceedings of the Indian Academy of Sciences-Section A*, volume 82 of number 4, pages 121–141. Springer India New Delhi, 1975.

[41] RG Rastogi. Westward equatorial electrojet during daytime hours. *Journal of geophysical research*, 79(10):1503–1512, 1974.

[42] G Manju, R Sridharan, Sudha Ravindran, MK Madhav Haridas, Tarun K Pant, P Sreelatha, and SV Mohan Kumar. Rocket borne in-situ electron density and neutral wind measurements in the equatorial ionosphereâresults from the january 2010 annular solar eclipse campaign from india. *Journal of atmospheric and solar-terrestrial physics*, 86:56–64, 2012.

[43] Chia-Hung Chen, Jann-Yenq Liu, K Yumoto, Chien-Hung Lin, and Tzu-Wei Fang. Equatorial ionization anomaly of the total electron content and equatorial electrojet of ground-based geomagnetic field strength. *Journal of Atmospheric and Solar-Terrestrial Physics*, 70(17):2172–2183, 2008.

[44] Jingxiu Wang. Electric conductivity of lower solar atmosphere. In *International Astronomical Union Colloquium*, volume 141, pages 465–468. Cambridge University Press, 1993.

[45] Bela G Fejer and Astrid Maute. Equatorial ionospheric electrodynamics. *Ionosphere dynamics and applications*:159–183, 2021.

[46] RG Rastogi. Longitudinal variation in the equatorial electrojet. *Journal of Atmospheric and Terrestrial Physics*, 24(12):1031–1040, 1962.

[47] MA Abdu, PAB Nogueira, JR Souza, IS Batista, SLG Dutra, and JHA Sobral. Equatorial electrojet responses to intense solar flares under geomagnetic disturbance time electric fields. *Journal of Geophysical Research: Space Physics*, 122(3):3570–3585, 2017.

[48] Claudia Stolle, Hermann Lühr, Martin Rother, and G Balasis. Magnetic signatures of equatorial spread f as observed by the champ satellite. *Journal of Geophysical Research: Space Physics*, 111(A2), 2006.

[49] Ramsingh, S Sripathi, Sreeba Sreekumar, S Banola, K Emperumal, P Tiwari, and Burudu Suneel Kumar. Low-latitude ionosphere response to super geomagnetic storm of 17/18 march 2015: results from a chain of ground-based observations over indian sector. *Journal of Geophysical Research: Space Physics*, 120(12):10–864, 2015.

[50] JP Schieldge, SV Venkateswaran, and AD Richmond. The ionospheric dynamo and equatorial magnetic variations. *Journal of Atmospheric and Terrestrial Physics*, 35(6):1045–1061, 1973.

[51] RT Marriott, AD Richmond, and SV Venkateswaran. The quiet-time equatorial electrojet and counter-electrojet. *Journal of geomagnetism and geoelectricity*, 31.

[52] Jeffrey J Love. Magnetic monitoring of earth and space. *Physics Today*, 61(2):31, 2008.

[53] INTERMAGNET contributors. International Real-time Magnetic Observatory Network — intermagnet.org. https://intermagnet.org. [Accessed 27-Jun-2023].

[54] Introduction to Geomagnetism | U.S. Geological Survey — usgs.gov. https://www.usgs.gov/programs/geomagnetism/introduction-geomagnetism. [Accessed 28-Jun-2023].

[55] Jürgen Matzka, Arnaud Chulliat, Mioara Mandea, Christopher C Finlay, and Enkelejda Qamili. Geomagnetic observations for main field studies: from ground to space. *Space Science Reviews*, 155:29–64, 2010.

[56] Magnetograms recording quiet times | U.S. Geological Survey — usgs.gov. https://www.usgs.gov/media/images/magnetograms-recording-quiet-times. [Accessed 06-Jul-2023].

[57] Achim Morschhauser, Gabriel Brando Soares, Jürgen Haseloff, Oliver Bronkalla, José Protásio, Katia Pinheiro, and Jürgen Matzka. The magnetic observatory on tatuoca, belém, brazil: history and recent developments. *Geoscientific Instrumentation, Methods and Data Systems*, 6(2):367–376, 2017.

[58] Achim Morschhauser, Gabriel Brando Soares, Jürgen Haseloff, Oliver Bronkalla, José Protásio, Katia Pinheiro, and Jürgen Matzka. The magnetic observatory on tatuoca, belém, brazil: history and recent developments. *Geoscientific Instrumentation, Methods and Data Systems*, 6(2):367–376, 2017.

[59] Marlos Goes, Gustavo Goni, Verena Hormann, and Renellys C Perez. Variability of the atlantic off-equatorial eastward currents during 1993–2010 using a synthetic method. *Journal of Geophysical Research: Oceans*, 118(6):3026–3045, 2013.

[60] C Manoj, Hermann Lühr, S Maus, and N Nagarajan. Evidence for short spatial correlation lengths of the noontime equatorial electrojet inferred from a comparison of satellite and ground magnetic data. *Journal of Geophysical Research: Space Physics*, 111(A11), 2006.

[61] The magnetic observatory on Tatuoca, BelxE9;m, Brazil: history and recent developments - ProQuest — proquest.com. https://www.proquest.com/openview/b5e1a5858fda20358a4026eb6015fc74/1?pq-origsite=gscholar&cbl=2037683. [Accessed 06-Jul-2023].

[62] Alex T Chartier, JD Huba, and Cathryn N Mitchell. On the annual asymmetry of high-latitude sporadic f. *Space Weather*, 17(11):1618–1626, 2019.

[63] Francisco Azpilicueta and Claudio Brunini. A new concept regarding the cause of ionosphere semiannual and annual anomalies. *Journal of Geophysical Research: Space Physics*, 116(A1), 2011.

[64] RuiPing Ma, JiYao Xu, WenBin Wang, GuangMing Chen, Wei Yuan, JiuHou Lei, Alan G Burns, and GuoYing Jiang. Characteristics and mechanisms of the annual asymmetry of thermospheric mass density. *Science China Earth Sciences*, 58:540–550, 2015.

[65] Yosuke Yamazaki, K Yumoto, T Uozumi, S Abe, MG Cardinal, D McNamara, R Marshall, BM Shevtsov, and SI Solovyev. Reexamination of the sq-eej relationship based on extended magnetometer networks in the east asian region. *Journal of Geophysical Research: Space Physics*, 115(A9), 2010.

[66] Hermann Lühr, Patrick Alken, and Yun-Liang Zhou. The equatorial electrojet. *Ionosphere Dynamics and Applications*:281–299, 2021.

[67] NSA Hamid, H Liu, T Uozumi, A Yoshikawa, and NMN Annadurai. Peak time of equatorial electrojet from different longitude sectors during fall solar minimum. In *Journal of Physics: Conference Series*, volume 852 of number 1, page 012015. IOP Publishing, 2017.

[68] Hui Wang, Zhichao Zheng, Kedeng Zhang, and Wenbin Wang. Influence of nonmigrating tides and geomagnetic field geometry on the diurnal and longitudinal variations of the equatorial electrojet. *Journal of Geophysical Research: Space Physics*, 125(6):e2019JA027631, 2020.

[69] Alemayehu Mengesha Cherkos et al. Solar flux effects on the variations of equatorial electrojet (eej) and counter-electrojet (cej) current across the different longitudinal sectors during low and high solar activity. *Journal of Astronomy and Space Sciences*, 40(2):45–57, 2023.

[70] LiBo Liu, WeiXing Wan, YiDing Chen, and HuiJun Le. Solar activity effects of the ionosphere: a brief review. *Chinese Science Bulletin*, 56:1202–1211, 2011.